

Recent Developments in Reversible CO₂ Hydrogenation and Formic Acid Dehydrogenation over Molecular Catalysts

Sanjeev Kushwaha,⁺ Jayashree Parthiban,⁺ and Sanjay Kumar Singh*Cite This: *ACS Omega* 2023, 8, 38773–38793

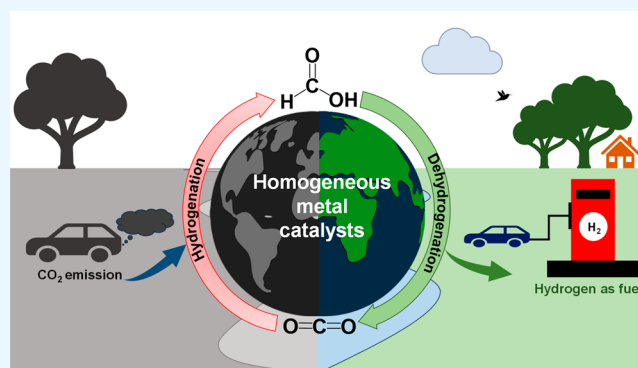
Read Online

ACCESS |

Metrics & More

Article Recommendations

ABSTRACT: Carbon dioxide (CO₂), a valuable feedstock, can be reutilized as a hydrogen carrier by hydrogenating CO₂ to formic acid (FA) and releasing hydrogen by FA dehydrogenation in a reversible manner. Notably, FA is liquid at room temperature and can be stored and transported considerably more safely than hydrogen gas. Herein, we extensively reviewed transition-metal-based molecular catalysts explored for reversible CO₂ hydrogenation and FA dehydrogenation. This Review describes different approaches explored for carbon-neutral hydrogen storage and release by applying CO₂ hydrogenation to FA/formate and the subsequent release of H₂ by the dehydrogenation of FA over a wide range of molecular catalysts based on noble and non-noble metals. Emphasis is also placed on the specific catalyst-to-substrate interaction by highlighting the specific role of the catalyst in the CO₂ hydrogenation–FA dehydrogenation pathway.



INTRODUCTION

The exponential growth of the global population has led to an increased demand for energy, resulting in a significant increase in the consumption of fossil fuels. Consequently, a substantial amount of greenhouse gases, including CO₂, has been emitted into the atmosphere. According to the Global Carbon Update of 2021, annual CO₂ emissions have surged from 11 billion tons in the 1960s to 35 billion tons in the 2010s. Consequently, the atmospheric CO₂ concentration has also increased from 317 ppm in 1960 to 424 ppm in 2023. The escalated CO₂ content in the atmosphere has catastrophic effects, including global temperature increases, melting glaciers, rising sea levels, and ocean acidification (by 30%), which continued further may disrupt the natural balance. Despite the negative implications, CO₂ is a useful and renewable C1 source that can be used for the production of useful chemicals such as methanol, formic acid, methane, and others, hence providing an opportunity to tackle the global issue of rising CO₂ levels in the atmosphere.¹ Notably, the hydrogenation of CO₂ to formic acid (FA) has gained more attention, as FA is an essential organic chemical feedstock with diverse applications in many fields, including agriculture, pharmaceutical, leather, and textile industries.² Hence, utilizing CO₂ as a hydrogen carrier via hydrogenation resulted in the formation of FA, and further dehydrogenation of FA generates hydrogen, while the CO₂ released is reused to close the carbon cycle. It is worth noting that the direct hydrogenation of CO₂ to FA in the gaseous phase, CO₂(g) + H₂(g) ⇌ HCOOH(l), is thermodynamically

unfavorable ($\Delta G^\circ = 32.8$ kJ/mol). However, when CO₂ hydrogenation is conducted in an aqueous phase with the addition of a base or amine, CO₂(aq) + H₂(aq) + NH₃(aq) ⇌ HCOO⁻(aq) + NH₄⁺(aq), the reaction becomes energetically favorable ($\Delta G^\circ = -35.4$ kJ/mol). Nevertheless, the benefit of the free energy gain to produce FA from H₂(aq) and CO₂(aq) is only 4 kJ/mol, suggesting that the equilibrium toward FA is only slightly favorable. Further, performing catalytic hydrogenation of CO₂ under neutral or acidic conditions resulted in lower activity. Thus, basic conditions are often employed for the hydrogenation, taking advantage of the stability of a formate salt being higher than that of FA.³

With the developing strategy of finding an alternate greener energy source for reducing CO₂ emissions in the environment, hydrogen has emerged as a strong contender for a carbon-free energy carrier, particularly for mobile applications when paired with proton-exchange membrane fuel cells.⁴ However, the practical use of hydrogen is limited by storage and delivery issues, which have led to the use of liquid organic hydrogen carriers (LOHCs) as they are easy to handle, store, and

Received: July 21, 2023

Accepted: September 27, 2023

Published: October 13, 2023



Table 1. Molecular Catalysts for Catalytic CO₂/(Bi)carbonate Hydrogenation and FA Dehydrogenation

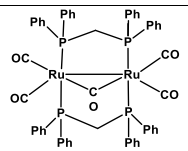
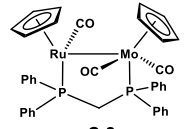
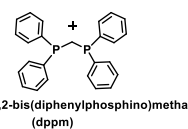
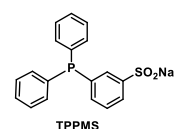
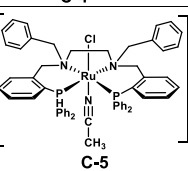
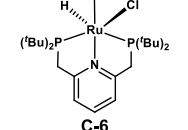
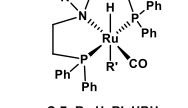
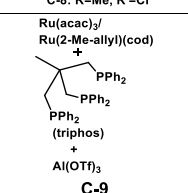
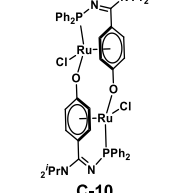
Catalysts	CO ₂ /(bi)carbonate hydrogenation							FA dehydrogenation					Ref.
	Substrate	pCO ₂ /pH ₂ (bar)	Additives	Solvent	T (°C)	TON	TOF (h ⁻¹)	FA (mmol)	Solvent	T (°C)	TON	TOF (h ⁻¹)	
 C-1	CO ₂	35/35	NEt ₃	CH ₃ OCH ₃	25	2.16 × 10 ³	103	10.5	CH ₃ OC H ₃	25	-	500	11
 C-2	CO ₂	30/30	NEt ₃	C ₆ H ₆	120	43	-	0.0251	THF-d ₆	80	-	-	12
[RuCl ₂ (benzene)] ₂  1,2-bis(diphenylphosphino)methane (dppm) C-3	NaHCO ₃ CO ₂	-/80 30/50	- LiOH	H ₂ O/THF	70	1.11 × 10 ³ 1.75 × 10 ³	- -	20 (HCOONa)	H ₂ O/DM F	60	2.0 × 10 ³	-	13
[RuCl ₂ (mTPPMS)] ₂  TPPMS C-4	HCO ₃ Na	-/100	-	H ₂ O	83	-	-	1.32 (HCOONa)	H ₂ O	80	1.20 × 10 ²	-	14
 C-5	CO ₂	70/70	DBU	-	100	5.6 × 10 ³	-	5	Toluene	100	-	-	15(a)
 C-6	CO ₂	10/30	DBU	DMF	120	2.0 × 10 ⁵	1.1 × 10 ⁶ (initial)	-	DMF	90	3.26 × 10 ⁵	2.57 × 10 ⁵	15(b)
 C-7: R = H, R' = HBH ₃ C-8: R = Me, R' = Cl	CO ₂	30/30	NaOH	THF /H ₂ O	76	1.16 × 10 ³	232	20 (HCOONa)	Dioxane /H ₂ O	70	5.0 × 10 ³	208	16
 C-9	CO ₂	40/40	-	Dioxane /H ₂ O	70	750	-	9	Dioxane /H ₂ O	90	2.0 × 10 ⁴	1.92 × 10 ³	17
 C-10	CO ₂	30/30	-	DMSO	60	160	-	2.65	DMSO	90	95	202 (initial)	18(a)

Table 1. continued

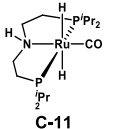
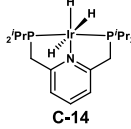
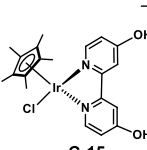
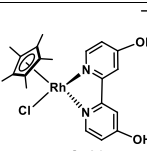
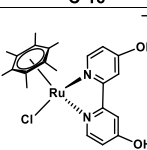
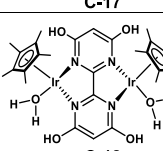
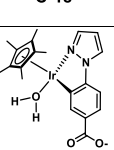
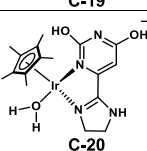
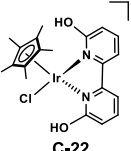
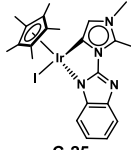
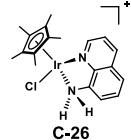
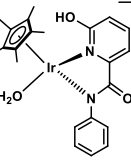
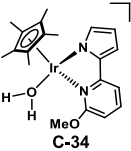
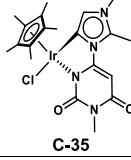
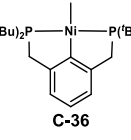
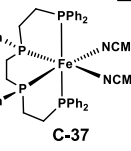
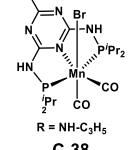
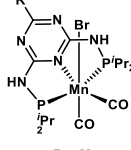
Catalysts	CO ₂ /(bi)carbonate hydrogenation							FA dehydrogenation					Ref.
	Substrate	pCO ₂ /pH ₂ (bar)	Additives	Solvent	T (°C)	TON	TOF (h ⁻¹)	FA (mmol)	Solvent	T (°C)	TON	TOF (h ⁻¹)	
 C-11	CO ₂	10/20	-	EMIM OAc	25	209	11	13.25	BMIM OAc	80	1.8× 10 ⁷	1.1 ×10 ⁴	18(b)
 C-14	CO ₂	40/40	KOH	H ₂ O /THF	200	3.5 ×10 ⁶	7.3 ×10 ⁴	5	^t BuOH /THF	80	5.0 ×10 ³	1.2 ×10 ³	19
 C-15	CO ₂	5/5	KOH	H ₂ O	80	1.1 ×10 ⁴	5.1 ×10 ³ (Initial)	-	-	-	-	-	20
 C-16	CO ₂	5/5	KOH	H ₂ O	80	1.2 ×10 ³	1.6 ×10 ² (Initial)	10	H ₂ O	60	3.8 ×10 ³	1.34 ×10 ² (Initial)	20
 C-17	CO ₂	5/5	KOH	H ₂ O	80	5.4 ×10 ³	92 (Initial)	10	H ₂ O	60	3.7 ×10 ³	94 (Initial)	20
 C-18	CO ₂	20/20	KHCO ₃	H ₂ O	50	1.53 ×10 ⁵	1.57 ×10 ⁴ (initial)	20	H ₂ O	80	3.0 ×10 ⁵	1.58 ×10 ⁵ (initial)	21
 C-19	CO ₂	1/1	K ₂ CO ₃	H ₂ O	30	>100	6.8	5	H ₂ O	25	3.13 ×10 ²	1.88 ×10 ³ (Initial)	22
 C-20	CO ₂	0.5/0.5	KHCO ₃	H ₂ O	25	7.28 ×10 ³	106 (Initial)	20	H ₂ O	60	2.9 ×10 ⁴	5.69 ×10 ⁴ (Initial)	23
 C-22	CO ₂	20/20	NaHCO ₃	H ₂ O	115	2.4 ×10 ³	130	25	H ₂ O	60	>3.5 ×10 ³	1.2 ×10 ³	24
 C-25	CO ₂	1/1	KOH	H ₂ O	30	-	58	40	H ₂ O	90	3.33 ×10 ³	1.0× 10 ⁵ (Initial)	25
	K ₂ CO ₃	-	-	H ₂ O		-	58						

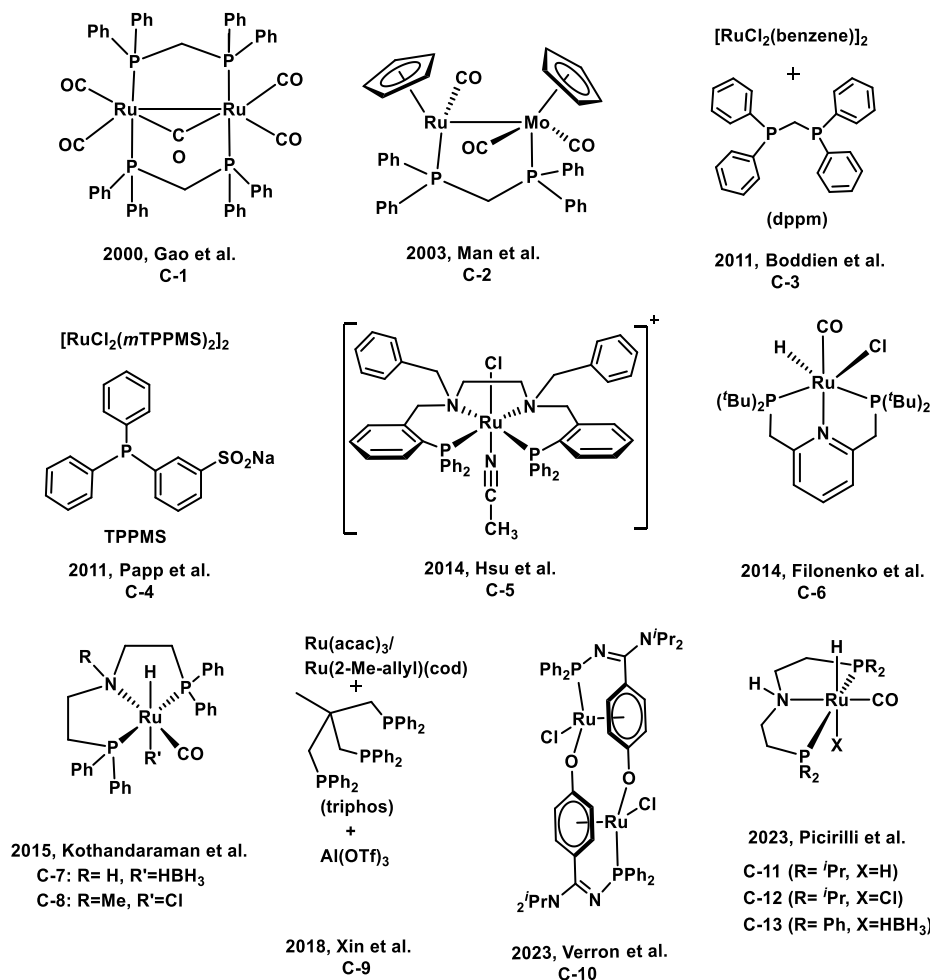
Table 1. continued

Catalysts	CO ₂ /(bi)carbonate hydrogenation							FA dehydrogenation					Ref.
	Substrate	pCO ₂ /pH ₂ (bar)	Additives	Solvent	T (°C)	TON	TOF (h ⁻¹)	FA (mmol)	Solvent	T (°C)	TON	TOF (h ⁻¹)	
 C-26	CO ₂	5/5	KOH	H ₂ O	80	6.02 × 10 ³	-	50	H ₂ O	100	3.11 × 10 ²	933	26
 C-30	CO ₂	0.05/0.05	NaHCO ₃	H ₂ O	25	-	198	10	H ₂ O	60	-	1.42 × 10 ⁴	27
 C-34	CO ₂	0.5/0.5	CsOH	MeOH/H ₂ O	25	-	29	4	H ₂ O	90	2.3 × 10 ³	4.59 × 10 ⁴	28
 C-35	CO ₂	30/30	KOH	H ₂ O	60	1.66 × 10 ⁴	-	6.89	H ₂ O	80	5.89 × 10 ³	7.06 × 10 ⁴ (Initial)	29
 C-36	NaHCO ₃	-/55	-	MeOH	150	3.04 × 10 ³	-	26	Propylene carbonate	80	626	209	30(a)
 C-37	NaHCO ₃	-/30	-	CH ₃ OH	80	766	-	5.3 × 10 ³	Propylene carbonate	60	6.06 × 10 ³	1.74 × 10 ³ (Initial)	30(b)
 C-38 R = NH-C ₂ H ₅	CO ₂	20/60	Lysine	H ₂ O/THF	115	2.3 × 10 ⁵	-	5	H ₂ O/THF	90	2.9 × 10 ⁴	-	31(a)
 C-39 R = Me	KHCO ₃ K ₂ CO ₃	-/60 -/60	- Glutamic acid	H ₂ O/THF H ₂ O/THF	90 90	5.5 × 10 ⁴	-	5	H ₂ O/THF	90	-	-	31(b)

transport. Among them, FA, which contains a volumetric hydrogen content of 4.4 wt %, has attracted significant attention due to its potential as a highly promising fuel for portable devices, vehicles, and various energy-related applications. FA is a desirable choice for LOHCs due to its accessibility, comparatively low toxicity, and minimal danger of explosions or other hazardous mishaps. Pure H₂ gas cannot be achieved from FA because an equimolar amount of CO₂ is also produced during the process of releasing H₂, although this does not pose a barrier for the use of fuel cells.⁵ FA (>10%) is corrosive to skin and eyes, volatile, and at risk of exposure

through inhalation.⁶ Further, selective FA dehydrogenation can result in the production of pressurized hydrogen gas and CO₂, making it an attractive alternative to hydrogen storage and a promising solution for growing energy needs. Recently, a method for separating high-pressure hydrogen from the H₂/CO₂ mixture gas produced by the breakdown of FA was devised. An appreciably high yield (85%) of pure hydrogen was achieved through the gas–liquid separation process, making FA a more attractive hydrogen carrier.⁷

Although several homogeneous⁸ and heterogeneous⁹ catalytic systems have been thoroughly explored, it is essential to

Scheme 1. Ruthenium-Based Catalysts C1–C13 Explored for Reversible CO₂ Hydrogenation and FA Dehydrogenation

have efficient catalytic systems that can selectively convert CO₂ to FA through hydrogenation and then dehydrogenate the FA to release H₂ gas to harness the potential of complementary partners CO₂ and FA for the cycle of hydrogen storage and release. Among them, Ru-, Ir-, and Rh-based molecular catalysts have shown outstanding performance for reversible H₂ storage and release over the CO₂/FA cycle. This process offers the potential to create a H₂ storage/release system that can be controlled by a pH switch through the interconversion of CO₂ to FA and vice versa.⁸ However, the purification of the gas mixture (H₂ and CO₂ in 1:1 molar ratio) produced from FA is challenging. Recent reports inferred that the separation of H₂ from H₂/CO₂ mixed gas can be done by changing the gas mixture to gas–liquid phase under high-pressure conditions. Moreover, lowering the temperature enabled better separation while maintaining the high pressure. Recently, Iguchi et al. reported a separation method to obtain high-pressure H₂ with 85% purity at –51 °C after the gas–liquid separation process, endorsing the potential of FA as a promising hydrogen carrier.¹⁰ Here, in this Review, we briefly describe a wide range of noble- and non-noble metal-based catalysts reported for the reversible CO₂ hydrogenation and FA dehydrogenation (Table 1).

NOBLE METAL-BASED MOLECULAR CATALYST

Among the first few examples (Scheme 1), Gao et al. utilized a binuclear Ru-based catalyst [Ru₂(μ-CO)(CO)₄(μ-dppm)₂]

(1,2-bis(diphenylphosphino)methane, dppm) (C-1) for the interconversion of CO₂ and FA.¹¹ For CO₂ hydrogenation, the catalyst C-1 displayed a TON of 1050 (in 9 h) and a TOF of 116 h⁻¹ at 38 bar pressure p_{H₂}/p_{CO₂} (1:1) in acetone at room temperature in the presence of triethylamine. Further, doubling the pressure led to a significantly higher formate yield with TON and TOF values of 2160 and 103 h⁻¹, respectively, in 21 h. The catalyst C-1 also demonstrated the ability to dehydrogenate FA (0.35 M) with a TOF of 500 h⁻¹ at room temperature in acetone. Further, it was observed that increasing the catalyst amount led to an increase in the rate of FA dehydrogenation. Conversely, as the concentration of FA was increased, the rate of the reaction decreased. Notably, when the reaction was performed under more acidic conditions, the concentration of free-formate ions decreased significantly due to the formation of the adduct [(HCO₂)₂H].

Man et al. reported a Ru–Mo-based heterobimetallic [(η⁵-C₅H₅)Ru(CO)(μ-dppm)Mo(CO)₂(η⁵-C₅H₅)] complex (C-2) for reversible CO₂ hydrogenation and FA dehydrogenation.¹² Initially, at p_{H₂}/p_{CO₂} = 60 atm (1:1) in THF, a TON of 10 was achieved at 120 °C in 45 h. Changing the solvent from THF to benzene resulted in an increase in the TON to 43 in the presence of triethylamine. Under analogous catalytic conditions, the monometallic complexes were found to be inactive for CO₂ hydrogenation, which is attributed to the formation of strong dihydride species. Catalyst C-2 also exhibited activity for the complete dehydrogenation of FA.

Despite the relatively slow rate of FA dehydrogenation, monitoring the reaction by NMR spectroscopy suggests some interesting findings. A THF- d_8 solution containing catalyst C-2 and FA (25.1 μmol) within a sealed NMR tube was heated to 80 °C for 2.5 h, resulting in the formation of a formate complex, as confirmed by NMR.

Boddien et al. utilized a $[\{\text{RuCl}_2(\text{benzene})\}_2]$ precursor and 1,2-bis(diphenylphosphino)methane (dppm) (C-3) for the catalytic hydrogenation of CO_2 , carbonate, and bicarbonate in a basic solution.¹³ Initially, with 50 bar H_2 pressure, C-3 exhibited excellent efficiency for the hydrogenation of NaHCO_3 and KHCO_3 (without using CO_2) in THF/water (1:5 v/v), thereby producing 35% sodium formate with a TON of 807 and 23% potassium formate with a TON of 531 in 2 h at 70 °C. Moreover, increasing the amount of C-3 by twofold and extending the reaction time to 20 h resulted in a maximum TON of 1108. At 80 bar H_2 pressure, 96% conversion of NaHCO_3 to sodium formate (HCOONa) was achieved under analogous conditions. Furthermore, using CO_2 along with the inorganic bases $\text{Ca}(\text{OH})_2$, $\text{Mg}(\text{OH})_2$ and LiOH led to higher catalytic activity and enhanced the overall performance of the catalyst C-3. When LiOH and KOH were used, the conversion of 76% and 68% CO_2 , respectively, was observed at $p\text{H}_2/p\text{CO}_2 = 50:30$ bar. Moreover, C-3 also exhibited high activity for hydrogen production from formate in $\text{H}_2\text{O}/\text{DMF}$ (Figure 1),

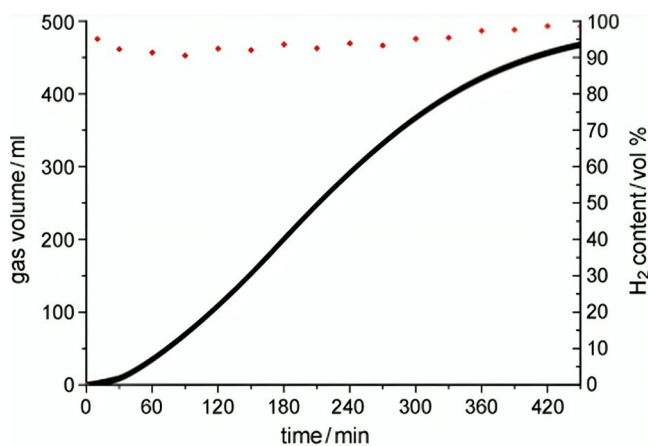


Figure 1. Hydrogen evolution curve and plot of the H_2 content (red dots) at 40 °C from a $\text{NaHCO}_2/\text{H}_2\text{O}$ mixture using 10 mmol $[\{\text{RuCl}_2(\text{benzene})\}_2]/6$ equiv of dppm (C-3) in 20 mL of DMF and 5 mL of H_2O . Reprinted with permission from ref 13. Copyright 2011 John Wiley and Sons.

where initial TOFs of 2923 and 2592 h^{-1} were achieved at 60 °C with lithium formate and HCOONa , respectively. Ammonium formate exhibited lower activity with a TOF of 126 h^{-1} , while magnesium formate and calcium formate displayed good H_2 liberation activities with TOF values of 420 and 770 h^{-1} , respectively. Further, investigating the effect of reaction temperatures on the hydrogen generation from HCOONa by lowering the reaction temperature to 25 °C led to a substantial decrease in the reaction rate of dehydrogenation in THF with a TOF of 19 h^{-1} . Complete dehydrogenation of HCOONa was achieved at 60 °C with a TON of 2000 in $\text{H}_2\text{O}/\text{DMF}$. To facilitate the formation of H_2 , excess water was used to provide additional protons, resulting in the selective dehydrogenation of formate. After H_2 release from formate, the pH of the reaction medium increases (basic), as the released CO_2 was captured in the basic solution

as bicarbonate, which was recovered as a solid after the reaction.

Papp et al. reported a charging–discharging hydrogen storage device using a $[\text{RuCl}_2(m\text{-tppms})_2]_2$ catalyst (C-4) containing a sodium diphenylphosphinobenzene-3-sulfonate (tppms) ligand.¹⁴ A TOF of 9600 h^{-1} was observed for the hydrogenation of bicarbonate at 80 °C under $p\text{H}_2$ of 60 bar and $p\text{CO}_2$ of 35 bar.^{14a} Similarly, the C-4 catalyst also displayed good activity for the dehydrogenation of sodium formate at 80 °C with a TON of 120 in 1 h, corresponding to a 47% conversion of formate. Further, the hydrogen storage and release cycles were performed in a sapphire NMR tube, where 90% conversion of aqueous sodium bicarbonate was observed at 100 bar H_2 and 83 °C. However, releasing H_2 pressure and heating the formed formate at 83 °C resulted in the dehydrogenation of formate, and the catalytic cycle was continued for three consecutive cycles. Moreover, the decomposition of formate decreased significantly when the conversion reached approximately 40–50%. As a result, only half of the H_2 storage capacity could be effectively utilized.^{14b}

Hsu et al. developed a rechargeable hydrogen battery using $[\text{Ru}(\text{Cl})(\text{CH}_3\text{CN})(\text{PNNP})][\text{PF}_6]$ catalyst (C-5) in the presence of DBU as base at 70 bar H_2 at 100 °C in 4 h, which efficiently reduced CO_2 to the corresponding DBU salt with a high TON of 5600.^{15a} Catalyst C-5 also catalyzed the dehydrogenation of formate salts of DBU at 100 °C. However, when the reaction temperature was decreased, the formate dehydrogenation rate also decreased. Notably, using toluene as the additive increased the rate of formate dehydrogenation, while pentafluorophenol had a minimal effect. The C-5 based catalytic system worked well for the five consecutive cyclic hydrogenation–dehydrogenation processes using dry ice and DBU, with an initial H_2 pressure of 70 bar at 100 °C (for hydrogenation), while heating the resulting solution at 100 °C resulted in the release of H_2 gas in the absence of any external pressure (Figure 2).

Filonenko et al. developed a Ru-PNP pincer catalyst (C-6) for CO_2 hydrogenation and FA dehydrogenation (Scheme 2).^{15b} Hydrogenation of CO_2 was carried out under various H_2/CO_2 molar ratios with a total pressure of 40 bar. The reaction exhibited high efficiency when DMF was used as the solvent along with DBU as the base, where initially, at 40 bar $p\text{H}_2/p\text{CO}_2$ (1:1), a TOF of 36 000 h^{-1} at 65 °C was achieved. Increasing the H_2 amount (40 bar, H_2/CO_2 ratio of 3:1) resulted in an increased TOF of up to 65 000 h^{-1} . Further increasing the temperature to 120 °C led to an increase in TOF to 1 100 000 h^{-1} . In DMF, catalyst C-6 also exhibited excellent stability and the highest reaction rate for FA dehydrogenation. Notably, the reaction followed first-order behavior with respect to formate in the presence of DBU. This suggested that the base promoters actively participate in the elementary steps of the catalytic reaction. With triethylamine (Et_3N), a maximum TOF of 257 000 h^{-1} and TON of 326 500 was achieved at 90 °C in DMF, suggesting the significant promotional effect of Et_3N on FA dehydrogenation.

They further explored the cyclic CO_2 hydrogenation and FA dehydrogenation by employing alternative loading procedures involving high (40 bar) and low (5 bar) pressures (H_2/CO_2 1:1) in DMF/DBU (6:1 v/v) at 65 °C. They observed complete hydrogen liberation within an hour, during which the rate of gas evolution reached its peak, achieving a TOF exceeding 150 000 h^{-1} (Figure 3). Advantageously, these cyclic operations were carried out without any need to introduce

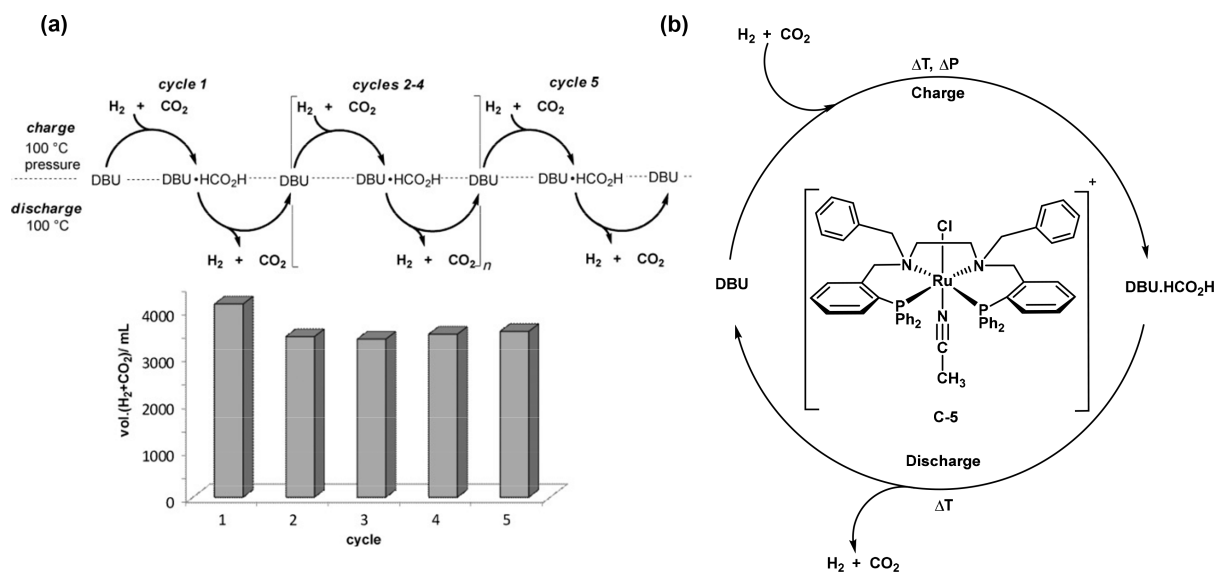
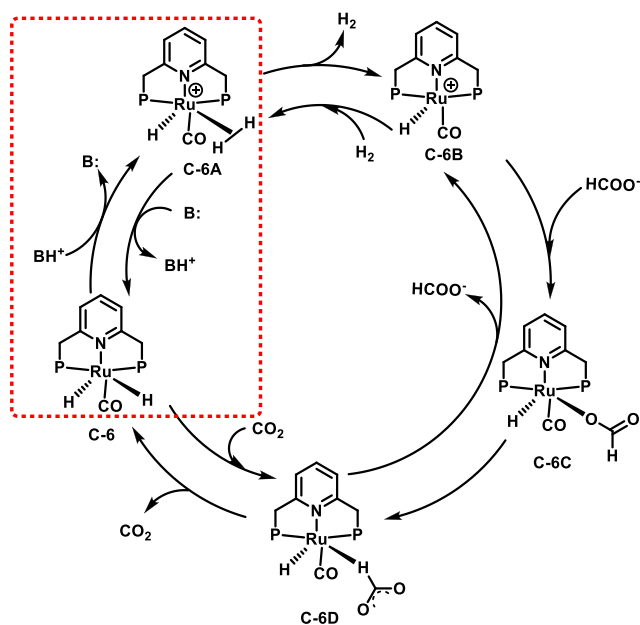


Figure 2. (a) Charging and discharging cycles of the H₂ battery and (b) pathway for the reversible H₂ storage and release over CO₂ over the catalyst C-5. Reprinted with permission from ref 15a. Copyright 2014 WILEY-VCH Verlag GmbH.

Scheme 2. Catalytic Pathway for CO₂ Hydrogenation and FA Dehydrogenation over Ru-PNP Catalyst C-6^a



^aReprinted with permission from ref 15b. Copyright 2014 WILEY-VCH Verlag GmbH.

additional base between cycles and without catalyst deactivation throughout the process.

Kothandaraman et al. presented a novel approach for the reversible hydrogen storage and release system, which relied on the equilibrium between CO₂ (HCO₃⁻) and H₂, as well as the formate species.¹⁶ This method utilized carefully characterized and readily accessible Ru-PNP complex-based catalysts. The system is amine-free, efficient, and reversible, with over 90% yield in both the hydrogenation and dehydrogenation directions (Scheme 3). They used the Ru-MACHO-BH catalyst (C-7) for efficient hydrogenation of CO₂, where MACHO ligands at HN(CH₂CH₂PR₂)₂, with isopropyl or

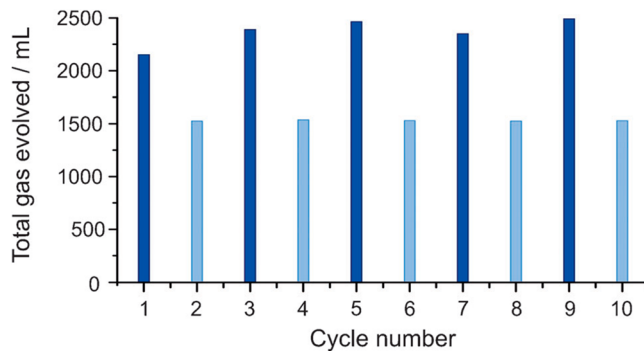
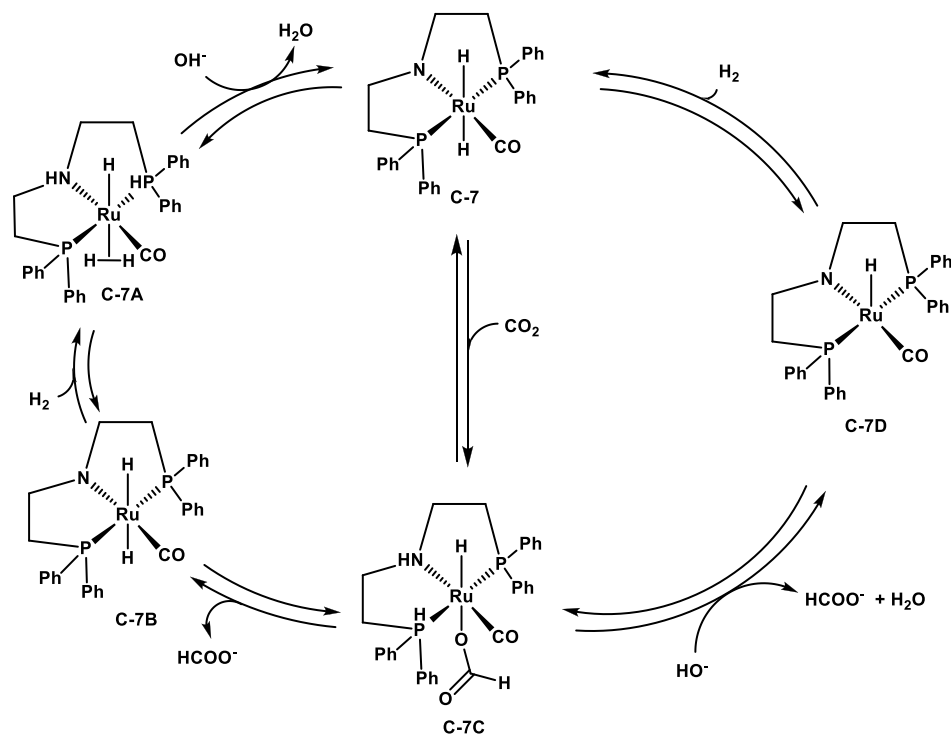


Figure 3. Total gas evolution in the H₂ storage–release cycles over the catalyst C-6 in DMF/DBU. Storage was performed at 65 °C under 40 (dark bars) and 5 bar (light bars) H₂/CO₂ = 1:1. Release was performed after decompression of the system at 65 °C followed by heating to 90 °C (conditions: DMF/DBU = 30:5 mL, 1.42 mmol catalyst). Reprinted with permission from ref 15b. Copyright 2014 WILEY-VCH Verlag GmbH & Co. KGaA, Weinheim.

phenyl as the R group. Treating hydroxides of Na, K, and Li in the presence of C-7 at 60 bar p_{H₂}/p_{CO₂} (1:1) resulted in the formation of sodium formate (93%), potassium formate (83%), and lithium formate (80%). Moreover, C-8 also hydrogenated CO₂ to yield formate (84%) in the presence of NaOH with a TON of 10 775 and TOF of 1096 h⁻¹ in 10 h using p_{H₂}/p_{CO₂} (61:20 bar) in 1,4-dioxane/H₂O as base at 70 °C. The catalysts C-7 and C-8 also displayed high activity for the dehydrogenation of sodium formate, with initial TOFs of 286 (at 69 °C) and 430 h⁻¹ (at 68 °C), respectively. Further, initial TOFs of 437 and 290 h⁻¹ were observed for lithium formate and potassium formate dehydrogenation at 70 and 71 °C, respectively, using the catalyst C-7.

The reversibility of the CO₂ hydrogenation system in the presence of C-7 was demonstrated by performing the dehydrogenation of *in situ* formed formate. The reaction mixture was initially hydrogenated to formate and then dehydrogenated to H₂ and CO₂ by a pressure swing at different temperatures. The system showed a continuous pressure increase during dehydrogenation, indicating the

Scheme 3. Catalytic CO₂ Hydrogenation and FA Dehydrogenation Cycle over Ru-PNP Catalyst C-7^a

^aReprinted with permission from ref 16. Copyright 2015 WILEY-VCH Verlag GmbH.

generation of H₂ and CO₂ from sodium formate. Notably, solar thermal energy was used during the hydrogenation and dehydrogenation steps over the studied catalytic system. The volumetric storage capacity of this system, 16.4 L of H₂ per liter of solution, is comparable to the best reported in the literature for amine-free pressure swing hydrogen-storage systems to date. However, in this system, no solvent change or external pH control was necessary to reverse the reaction, as the pH change occurs spontaneously. Consecutive reversible cycles of CO₂ hydrogenation (charging) and formate dehydrogenation (discharging) were performed to achieve the consistent performance of catalyst C-7 without any significant loss in activity. The release of a CO-free H₂/CO₂ gas mixture suggests the potential application of the C-7 catalyst in hydrogen batteries and hydrogen fuel cells. The catalyst C-7 exhibited a cumulative TON of 11 500 during the six consecutive hydrogenation–dehydrogenation cycles, demonstrating the stability and efficiency of this catalytic system for hydrogen storage.

Xin et al. also reported the successful application of a Ru-triphos complex (C-9) combined with Al(OTf)₃ for the reversible hydrogen storage and release over CO₂–FA cycle.¹⁷ To achieve exceptional performance, a Lewis acid, Al(OTf)₃, was utilized in a Ru-triphos complex (C-9) catalyst due to its ability to activate both the substrate and catalyst through a weak interaction. The process was observed to occur through two primary pathways: the first pathway involves promoting the formation of active cationic ruthenium species under acidic conditions, while the second involves accelerating the cleavage of polar C–O or C–N bonds through acid–base interactions. Under the conditions of 40 atm of both H₂ and CO₂, a mixture of 1,4-dioxane and water as the solvent, and using the catalyst precursors comprised of 0.1 mol % Ru(acac)₃, 0.1 mol % triphos, and 0.25 mol % Al(OTf)₃, FA was produced with 65%

conversion of CO₂ and a TON of 750 after 18 h at 70 °C. Treating NaHCO₃ with H₂ (2.8 bar) at 90 °C using the catalyst precursors comprised of 0.1 mol % Ru(acac)₃, 0.1 mol % triphos, and 0.1 mol % Al(OTf)₃ also resulted in the formation of HCOONa with 86% conversion after 10 h. Further, under pressure, the catalyst C-9 exhibited stable H₂ production from FA and was successfully recycled up to 14 runs with a maximum initial TOF of 1920 h⁻¹ and TON up to 20 000 (Figure 4). Surprisingly, when Al(OTf)₃ was introduced, kinetic studies revealed observable acceleration effects. In the process of FA dehydrogenation, the rate was

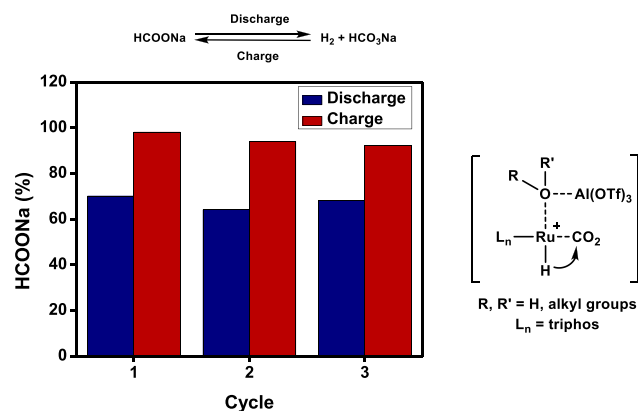


Figure 4. Sodium formate-based rechargeable hydrogen battery in the presence of C-9 catalyst. Reaction conditions are as follows: Both the charge and discharge reactions were performed in the sealed pressure tube using sodium formate (1 mmol), Ru(acac)₃ (1 mol %), triphos (1 mol %), Al(OTf)₃ (1 mol %), 1 mL of 1,4-dioxane, and 1 of mL H₂O at 90 °C. For charge reaction, 70 bar H₂ was used. Conversions were determined by ¹³C NMR.

enhanced twofold (TOF from 550 to 1200 h⁻¹) upon the incorporation of Al(OTf)₃. In order to understand the promotion effect of Al(OTf)₃ on the reaction mechanism, *in situ* NMR experiments were conducted. These experiments revealed that aluminum triflate activates both the precatalysts and FA by enhancing the activity of Ru–H species and modulating the polarity of the carbonyl group of FA through direct O–Al interactions, respectively, implying that the reaction proceed through a different mechanism as in the previously reported Ru-triphos complexes; no hydride signals were detected in the presence of organic base (Figure 4). Various organic solvents as well as mixtures of H₂O and organic solvents were found to be suitable for this reaction. However, the rate of hydrogen evolution was quite slow in the absence of sodium formate for FA dehydrogenation. The most efficient reaction was achieved by maintaining a HCOONa/FA ratio of 1:9 in the presence of 0.25 mol % Al(OTf)₃ in the H₂O/THF mixture.

Verron et al. reported a dimeric tethered π -coordinated-phenoxy ruthenium precatalyst (C-10) for reversible CO₂ hydrogenation and FA dehydrogenation in DMSO under base-free condition.^{18a} They observed higher activity for CO₂ hydrogenation at elevated pressure, where a TON of 105 was achieved at 60 bar *p*H₂/*p*CO₂ (1:1) as compared to a TON of 9 at 40 bar *p*H₂/*p*CO₂ (1:1) at 60 °C in DMSO. The highest TON of 160 was achieved at a pressure of 60 bar *p*H₂/*p*CO₂ (1:1) in 65 h. Additionally, exploring the effect of temperature showed that a higher TON of 114 was observed at 80 °C, but further increasing the temperature to 90 °C led to a decrease in the TON to 90, presumably due to reduced catalyst stability at higher temperatures. Notably, lower activity was observed for the reaction performed in a mixture of DMSO and water. For FA dehydrogenation, the catalyst C-10 (0.5 mol %), FA (2.4 M), and DMSO as the solvent were used to achieve a conversion of 95% with the highest TOF of 202 h⁻¹ in 20 min. Decreasing the catalyst loading to 0.25 mol % resulted in a high TON of 173 when the reaction time was extended, thereby highlighting the resilience of both C-10 and the active catalytic species. Doubling the FA concentration resulted in a slightly increased activity. Further, the capability of catalyst C-10 to generate high-pressure H₂ (up to 42 bar) was demonstrated, which is sufficient for to supply hydrogen to proton exchange membrane (PEM) fuel cells. Further, the catalytic tandem hydrogenation and dehydrogenation process was investigated in which initially the hydrogenation of CO₂ resulted in the formation of FA (0.4 mol L⁻¹). The FA solution was then subjected to dehydrogenation by heating, where ~94% of the expected gas volume was released within 40 min, demonstrating the successful base-free hydrogen storage and release cycle.

Piccirilli et al. explored Ru-PNP pincer complex [Ru(H)-(X)(CO)(PNP)] (PNP = bis(isopropyl- or phenyl)-ethylphosphinoamine) in ionic liquids (ILs) for reversible hydrogen storage and release over CO₂/FA system.^{18b} Ionic liquids possess greater advantages, such as low melting point, negligible vapor pressure, and high thermal and chemical stability, and act as a good CO₂ chemisorbents, making the hydrogenation process successful without the use of any additive. CO₂ hydrogenation over [Ru(H)₂(CO)(ⁱPrPNP)] (C-11) in 1-ethyl-3-methyl imiazolium acetate (EMIM OAc) under 30 bar *p*H₂/*p*CO₂ (2:1) resulted in the formation of FA (65 mol % FA/IL) with >95% conversion of CO₂ (TON of 209) in 18 h at 25 °C. Further investigation of various reaction

parameters showed that the IL trapped CO₂ efficiently, as it became viscous or solid at 25 °C, thereby requiring elevated partial H₂ pressure to overcome gas diffusion limitations into the IL in order to attain the high TON. As a result, 70 and 75 mol % FA/IL were achieved at 30 bar *p*H₂/*p*CO₂ (2:1) (with 0.5 mol % catalyst) and *p*H₂/*p*CO₂ (1:1) (with 0.2 mol % catalyst), respectively. On the other hand, 35 mol % FA/IL was achieved at 40 bar *p*H₂/*p*CO₂ (1:1) in the first recharge. However, upon reloading the system with 40 bar *p*H₂/*p*CO₂ (1:1), the FA yield was increased to 111% and 126% FA/IL with the second and third recharge, respectively. The FA space-time yield (STY) of 0.33 mol L⁻¹ h⁻¹ at 25 °C was increased to 1.03 mol L⁻¹ h⁻¹ at 80 °C. Moreover, the TON of 18 886 in 18 h at 80 °C further increased to 32 411 with the increase in pressure to 60 bar *p*H₂/*p*CO₂ (1:1). In order to perform the cyclic CO₂ hydrogenation and FA dehydrogenation, it was found that the equilibrium within the catalytic system could be influenced to favor either hydrogenation or dehydrogenation by controlling the pressure or temperature (Figure 5). When a temperature >60 °C was applied to a

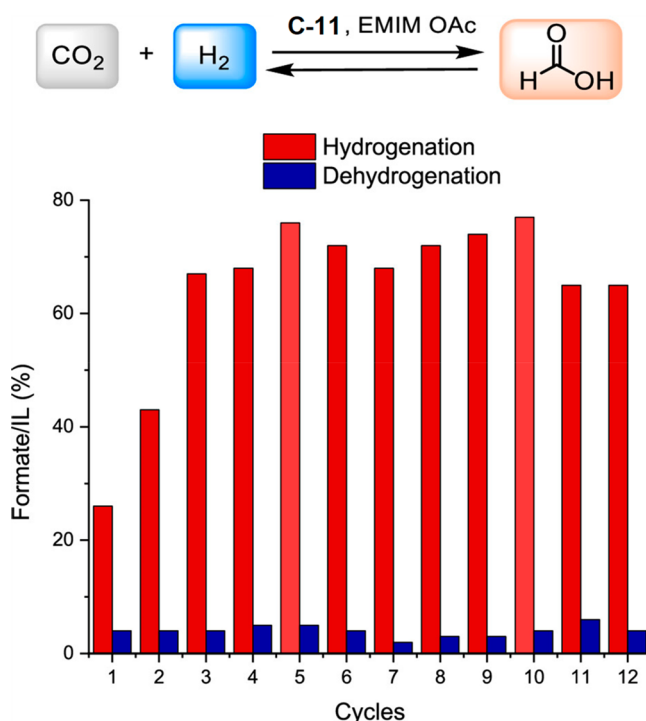
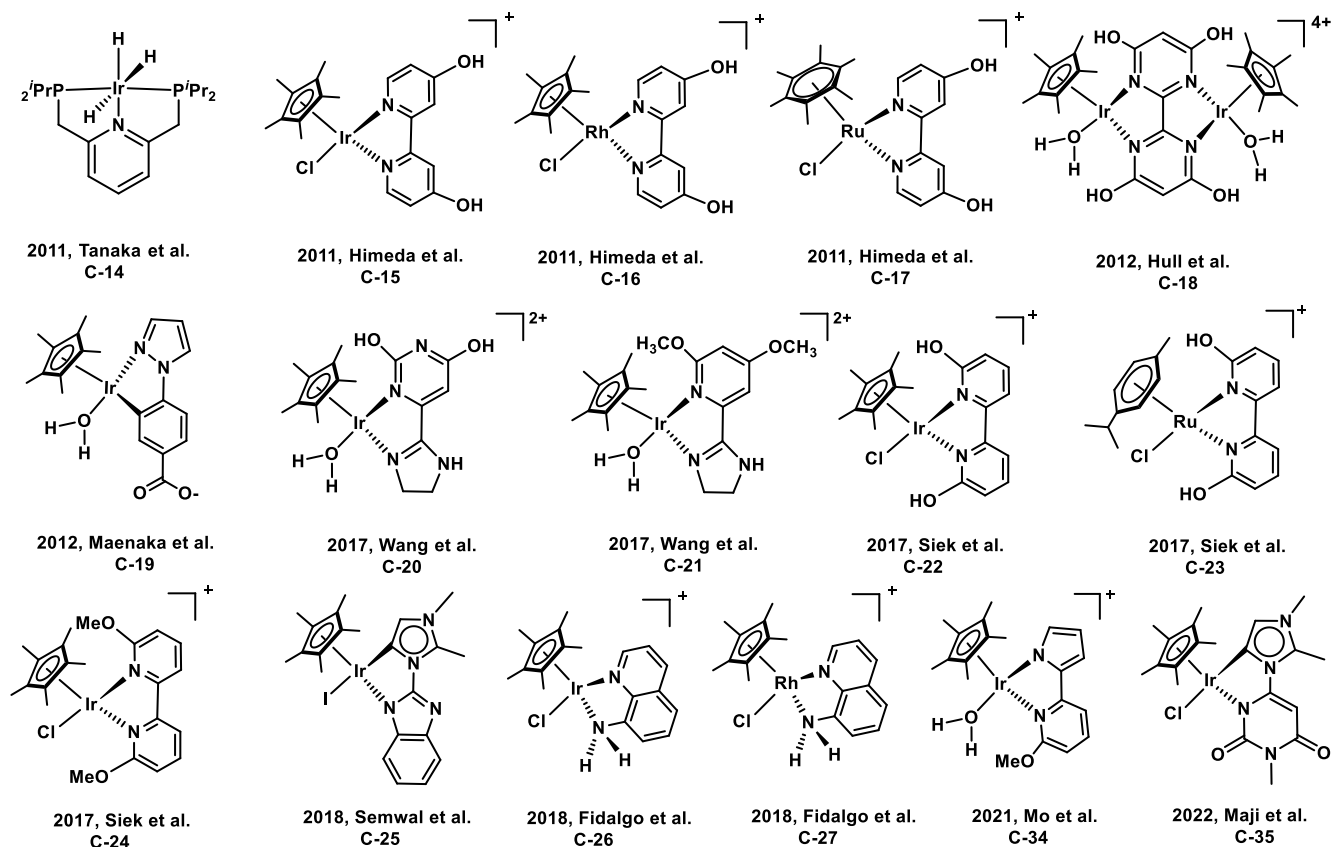


Figure 5. Cycles were applied to CO₂ hydrogenation experiments followed by hydrogen release. Reaction conditions are as follows: C-11 (0.07 mmol) and EMIM OAc (2 mL). For hydrogenation, 10:20 bar CO₂/H₂ was used at 25 °C for 18 h (red bars) or 72 h (lighter bars). For dehydrogenation, the reaction was performed at 95 °C for 4 h. Reprinted with permission from ref 18b. Copyright 2023 American Chemical Society.

mixture of FA/IL, a gas mixture containing CO₂ and H₂ (1:1 v/v) was released. This controlled process performed using C-11 catalyst (0.0013 M) in EMIM OAc led to a remarkable TON of 51 761 after 10 cycles. Similarly, the hydrogenation step was carried out at 25 °C over 18 or 72 cycles using 30 bar *p*H₂/*p*CO₂ (2:1). Subsequently, heating to 95 °C for 4 h favored the release of H₂ gas. Both C-11 and [Ru(H)(Cl)-(CO)(ⁱPrPNP)] (C-12) catalysts were found to be active for more than 13 cycles with no discernible signs of catalyst

Scheme 4. Ir/Rh/Ru-Based Catalysts C-14–C-35 Explored For Reversible CO₂ Hydrogenation and FA Dehydrogenation

deactivation. With **C-11** (0.07 mmol, 0.035 M), each hydrogenation step reached a saturation point at around 70 mol % FA/IL, whereas lower concentrations of **C-12** (0.05 mmol, 0.025 M) resulted in even higher FA/IL molar ratios (>100 mol %), leading to an overall TON of 7739 after 13 charge–discharge cycles with the detection of the traceable amount of CO. For FA dehydrogenation performed at temperatures below 100 °C with [Ru(H)(BH₄)(CO)-(PhPNP)] (**C-13**) in 1-butyl-3-methyl imiazolium acetate (EMIM OAc), a high TOF (11 000 h⁻¹) and TON (up to 18 000,000) were achieved after 112 days, inferring the excellent stability of the studied catalyst. Moreover, all these catalysts (**C-11**, **C-12**, and **C-13**) were extremely reliant on the rate of FA addition, where a FA/IL ratio of >3600 was required to achieve high turnover.

Tanaka et al. demonstrated an Ir-PNP-trihydride (**C-14**) as the most effective catalytic system for CO₂ hydrogenation and FA dehydrogenation (Scheme 4), where the studied catalytic process was tuned to achieve reversibility by employing a base, triethanolamine.¹⁹ Further studies showed that the strength of the base used and the pressure of H₂ and CO₂ play crucial roles in achieving higher catalytic activity. The catalyst **C-14** (0.010 μmol) works well in an aqueous KOH solution in the presence of THF at 120 °C with 80 bar p_{H₂}/p_{CO₂} (1:1), achieving 94% formate yield with a TON of 470 000. Decreasing the catalyst amount by ten times resulted in an increased TON of 3 500 000 and a TOF of 73 000 h⁻¹. A further increase in the base concentration led to a lower formate yield, while an enhanced catalytic activity was observed when a more polar solvent was used. DFT studies revealed two pathways for CO₂ hydrogenation: the depro-

tonation step and the hydrogenolysis step as the rate-determining steps.⁸ Further, for the dehydrogenation of FA or formate, a TON of 890 was achieved over catalyst **C-14**. Catalytic activity was greatly enhanced when triethylammonium formate was employed, with the initial TOF of 120 000 h⁻¹ at 80 °C. Performing FA dehydrogenation in ^tBuOH in the presence of Et₃N resulted in complete dehydrogenation of FA with a TON of 5000 at 80 °C.

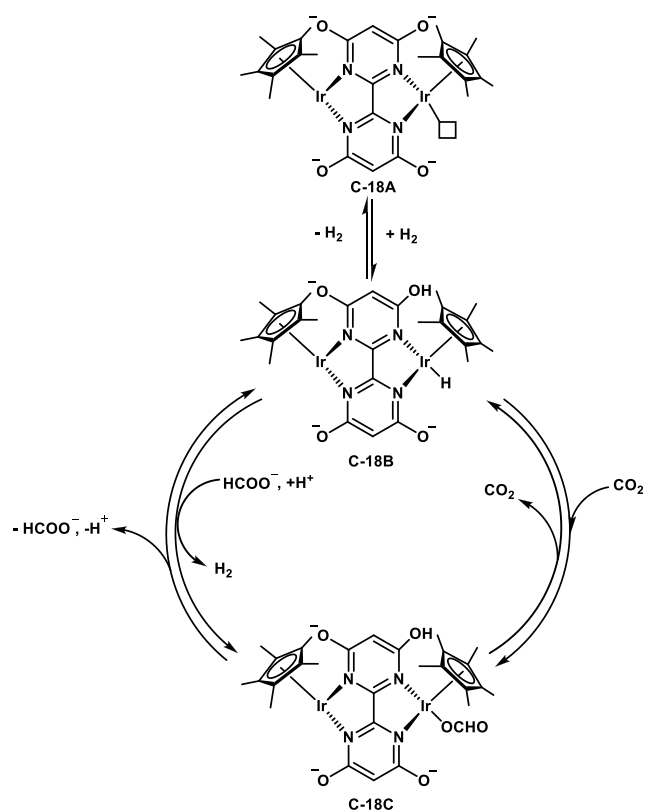
Himeda et al. explored 4,4'-dihydroxy-2,2'-bipyridine (4,4'-dhbp) ligated Cp*Ir (**C-15**), Cp*Rh (**C-16**), and (η⁶-C₆Me₆)Ru (**C-17**) catalysts for CO₂ hydrogenation, while the **C-16** and **C-17** catalysts were only explored for FA dehydrogenation.²⁰ CO₂ hydrogenation was performed at 80 °C in 1 M KOH solution at 10 bar p_{H₂}/p_{CO₂} (1:1) to achieve initial TOFs of 160 and 92 h⁻¹ and TONs of 1200 and 5400, respectively, for **C-16** and **C-17**. On the other hand, **C-15** exhibited the highest catalytic activity with an initial TOF of 5100 h⁻¹ and a TON of 11 000. Moreover, Cp*Rh (**C-16**) and (η⁶-C₆Me₆)Ru (**C-17**) catalysts were also explored for FA dehydrogenation to achieve moderate to poor catalytic activity (initial TOF values of 1340 h⁻¹ and 94 h⁻¹, respectively) at 60 °C. The significant catalytic activity was attributed to the electronic effect of oxyanions produced through the deprotonation of the -OH groups in the 4,4'-dhbp ligand.

Hull et al. also explored a proton-switchable Cp*Ir binuclear catalyst (**C-18**) for both CO₂ hydrogenation and FA dehydrogenation in aqueous medium.²¹ Initially, at p_{H₂}/p_{CO₂} = 1 bar (1:1), a TON of 7200 and an initial TOF of 64 h⁻¹ with the formation of 0.36 M formate were achieved at 25 °C. Upon the addition of 2 M KHCO₃, the formate yield was increased to 0.56 M, with an initial TOF of 70 h⁻¹. Further, by

increasing the temperature to 50 °C, an impressive TON of 153 000 under 40 bar $p_{\text{H}_2}/p_{\text{CO}_2}$ (1:1) was achieved, and a TOF of 53 800 h^{-1} was achieved at 80 °C under 50 bar $p_{\text{H}_2}/p_{\text{CO}_2}$ (1:1). The FA dehydrogenation performed under acidic conditions revealed that the catalyst **C-18** underwent intermediate protonation at pH 3.5 to release H_2/CO_2 (1:1) from an aqueous mixture of FA and HCOONa with an impressive initial TOF of 228 000 h^{-1} at 90 °C and a TON of 308 000 at 80 °C. Notably, the $-\text{OH}$ groups of bipyrimidine ligand were found to have a more pronounced impact on CO_2 hydrogenation as compared to that on FA dehydrogenation. The reversible hydrogen storage over catalyst **C-18** was achieved by tuning the pH of the reaction. The catalyst **C-18** catalyzed the hydrogenation of 2 M KHCO_3 under a constant gas flow of 10 bar $p_{\text{H}_2}/p_{\text{CO}_2}$ (1:1) to yield 0.48 M formate after 136 h at room temperature. After completion of the reaction, the solution was cooled and the pH was adjusted to 1.7 using H_2SO_4 (4 M) to protonate the catalyst. Further heating the solution in a glass autoclave to 50 °C generated H_2 gas by the dehydrogenation of formate. The cycle was repeated further by adjusting the pH for the hydrogenation of KHCO_3 . The pH-responsive $-\text{OH}$ moieties of the bipyrimidine ligand in **C-18** were responsible for showing the on and off H_2 storage properties. As a result, the system was recycled without catalyst isolation prior to use. Based on the free energy calculation, which was found to be consistent with the experimental data, the plausible reaction mechanism is proposed as follows: Initially, H_2 activation over the Cp^*Ir catalyst forms $\text{Ir}-\text{H}$ species ($\Delta G^\circ = -0.58 \text{ kcal mol}^{-1}$), followed by the CO_2 insertion into the $\text{Ir}-\text{H}$ species ($\Delta G^\circ = +8.4 \text{ kcal mol}^{-1}$). Finally, the formate formed was released with the regeneration of the $\text{Ir}-\text{H}$ species ($\Delta G^\circ = -9.4 \text{ kcal mol}^{-1}$) (Scheme 5). Therefore, the net free energy of the CO_2 hydrogenation reaction was found to be $-1.6 \text{ kcal mol}^{-1}$.

Maenaka et al. reported a Cp^*Ir catalyst (**C-19**) based on a $[\text{C},\text{N}]$ -cyclometalated pyrazole benzoic acid ligand for FA dehydrogenation and CO_2 hydrogenation by controlling the pH of the reaction mixture under ambient temperature and pressure.²² For the bicarbonate hydrogenation to formate, initially reactions were carried out by bubbling CO_2 in 0.1 M K_2CO_3 solution for 1 h at 30 °C, followed by H_2 and CO_2 bubbling (1:1 v/v) under ambient pressure and temperature at pH 7.5. As a result, formate was formed with good yields, with TOFs of 6.8 and 22.1 h^{-1} at 30 and 60 °C, respectively, in H_2O . It was found that at pH 8.8 the TOF reached its maximum value, and further increasing the pH led to a drop in the TOF. The catalyst **C-19** was found to effectively hydrogenate bicarbonate over carbonate. Hence, at pH 8.8, it was observed that the TOF increases linearly as the temperature and bicarbonate concentration both increase. The catalytic steps for the bicarbonate hydrogenation by H_2 were monitored by UV–visible spectroscopy, where the $\text{Ir}-\text{H}$ species ($\lambda_{\text{max}} = 340 \text{ nm}$) followed by the formate species ($\lambda_{\text{max}} = 430 \text{ nm}$) were formed by the interaction of $\text{Ir}-\text{H}$ and bicarbonate. The catalytic pathway for the interconversion between H_2 and FA involves two catalytic cycles: one in slightly basic water and the other in acidic solution. The hydrogenation process was performed in slightly basic water, where the initial formation of hydrido species was characterized by ^1H NMR spectrum, mass, and UV–vis absorption spectrum. The interaction with HCO_3^- leads to the formation of a formate species, which is subsequently released as

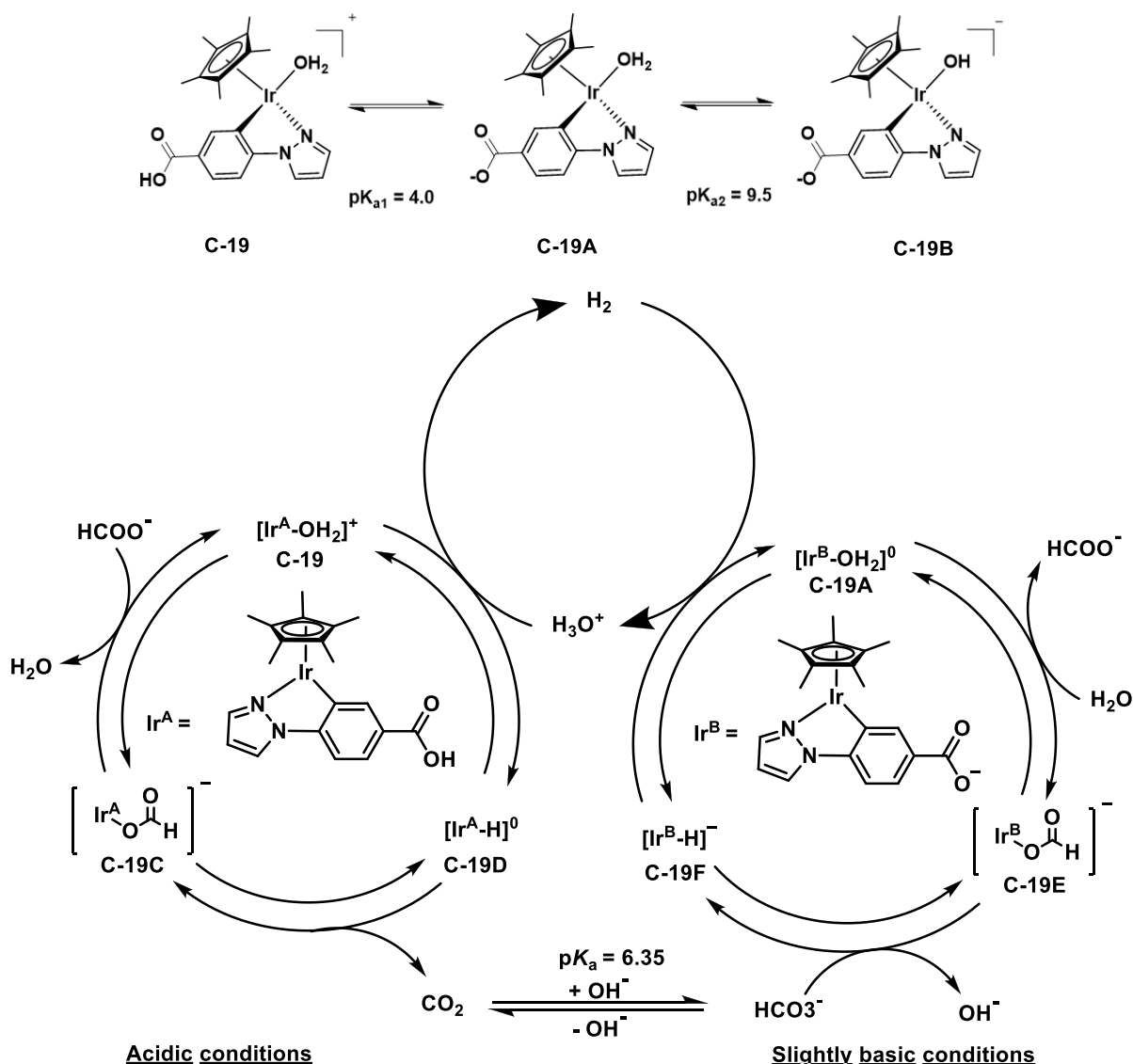
Scheme 5. Catalytic Pathway for CO_2 Hydrogenation and FA Dehydrogenation over the Cp^*Ir Catalyst **C-18^a**



^aReprinted with permission from ref 21. Copyright 2012 Springer Nature Limited.

HCOO^- . This process allows the regeneration of hydrido species, enabling the catalytic cycle to continue.

The catalyst **C-19** also catalyzed the FA dehydrogenation to H_2 and CO_2 (1:1 molar ratio) in acidic water, where a maximum TOF of 1880 h^{-1} was achieved at pH 2.8 at 25 °C. An increasing trend in TOF was observed with decreasing pH in the range from 9.0 to 2.8. Further decreases in pH below 2.8 resulted in the deactivation of the catalyst. This implies that **C-19** has a higher catalytic reactivity than the benzoate analogue (**C-19A**), which did not produce any hydrogen at pH 9.0 where **C-19** was fully converted to **C-19A** and (benzoate analogue with Ru -hydroxo) **C-19B** at 298 K. The rate-determining step (rds) in the catalytic FA dehydrogenation was suggested to be the β -hydrogen elimination of the Cp^*Ir formate species (**C-19C**) to form the Cp^*Ir hydrido species (**C-19D**), particularly at lower pH, due to the relatively high concentration of protons (Scheme 6). The kinetic deuterium isotope effect (KIE) for the dehydrogenation from deuterated FA (DCOOH) was investigated, and a KIE value of 4.0 was obtained at pH 2.8 and 25 °C. The catalytic activity of **C-19** increased linearly with increasing catalyst concentration, indicating its involvement in the rds of the catalytic FA dehydrogenation reaction. Furthermore, the reaction of formate with **C-19E** at pH 8.0 resulted in the formation of the hydrido species **C-19F** via formate **C-19E**. Under pH greater than 8.0, hydrido species **C-19F**, observed for the reaction of **C-19A** with FA, could not facilitate the proton-assisted production of H_2 due to the lower concentration of protons.

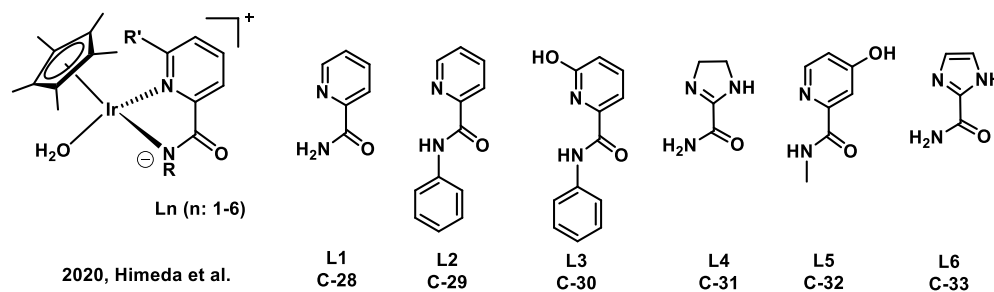
Scheme 6. CO₂ Hydrogenation and FA Dehydrogenation Catalyzed by Cp*Ir Catalyst C-19^a

^aAdapted figure from ref 22. Copyright 2012 Royal Society of Chemistry.

Wang et al. reported new pyridylimidazoline-based Cp*Ir catalysts, bearing two hydroxyl groups (C-20) and two methoxy groups (C-21) on the pyridyl moiety of the ligand, for CO₂ hydrogenation and FA dehydrogenation in water.²³ The catalyst C-20 demonstrated an initial TOF of 2600 h⁻¹ for CO₂ hydrogenation in a KHCO₃ (2 M) solution using 10 bar p_{H₂}/p_{CO₂} (1:1) at 50 °C. The catalyst C-20 bearing -OH groups exhibited superior catalytic activity to the catalyst C-21 bearing -OMe groups. At the same time, the effect of the substituent on the *ortho*, *meta*, and *para* positions played a vital role in achieving a higher TON. As a result, catalyst C-20 possessing two hydroxyl groups on positions *ortho* and *para* to the pyridine nitrogen performed exceptionally well, where a maximum TON of 7280 with 0.182 M formate yield was achieved after 336 h in the presence of NaOH (1 M) under 1 bar p_{H₂}/p_{CO₂} (1:1) at 25 °C. However, a higher formate yield (0.591 M) was achieved while 2 M KHCO₃ was used under the same reaction conditions. Notably, catalysts C-20 and C-21 also exhibited higher activity for the dehydrogenation of FA in water at 60 °C. Results suggested that catalyst C-21

exhibited a maximum TOF of 19 400 h⁻¹ at pH 1.7 but decreased activity at higher pH. Conversely, catalyst C-20 (-OH group) displayed significantly increased catalytic activity at pH 3.0, with a maximum TOF of 56 900 h⁻¹ and TON of 29000.

Siek et al. reported a comparative study on Cp*Ir (C-22) and (*p*-cymene)Ru (C-23) bearing proton-responsive dihydroxybipyridine (6,6'-dhbp) based ligands for CO₂ hydrogenation and FA dehydrogenation.²⁴ The catalysts [Cp*IrCl(6,6'-dhbp)]OTf (C-22) and [(*p*-cymene)RuCl(6,6'-dhbp)]OTf (C-23) were explored for CO₂ hydrogenation in the presence of NaHCO₃ (1 M) under 300 psi p_{H₂}/p_{CO₂} (1:1), resulting in TONs of 2400 and 2270 and TOFs of 130 and 126 h⁻¹, respectively, in 18 h at 115 °C. Ruthenium complexes being less active compared to iridium complexes led to the variation in the catalytic activity. The DFT study revealed that the enhanced catalytic performance of C-22 and C-23 was attributed to the secondary coordination sphere effect that aids the proton-responsive nature of hydroxy groups to form more electron-donating oxyanions during the catalytic reaction

Scheme 7. Iridium Metal-Based Catalysts C-28–C-33 Explored for Reversible CO₂ Hydrogenation and FA Dehydrogenation

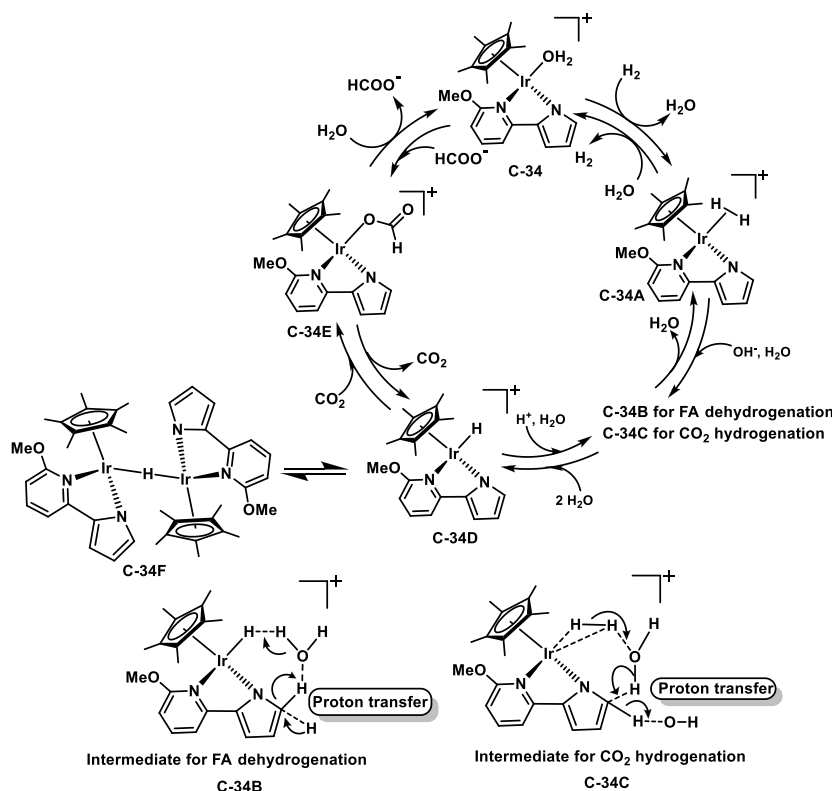
under basic conditions, thereby activating CO₂ for hydrogenation. Among the catalysts explored, C-22 demonstrated good activity for FA (1.02 M) dehydrogenation, yielding a TON of 3500 and a TOF of 1200 h⁻¹ at 60 °C for 3 h. In contrast, C-23 resulted in considerably lower TON (45) and TOF (15 h⁻¹) under analogous reaction conditions. Furthermore, investigations involving the catalyst bearing dimethoxybipyridine (dmbp) [Cp*IrCl(6,6'-dmbp)]OTf (C-24) were conducted; all other reaction conditions were kept constant while employing an incredibly low catalyst loading (0.0028 mol %). Remarkably, this adjustment resulted in a TOF approximately 2.8× higher (~3300 h⁻¹), coupled with a FA conversion of 29% at 3 h, and achieved a TON of 33 000 after 24 h. Initially, a 10-fold increase in the TOF was anticipated upon reducing the catalyst loading. However, it became apparent that at such low catalyst loading the reaction progressed at a slower pace, potentially due to the saturation of all available catalyst sites or interference from catalyst decomposition.

Semwal et al. reported a hybrid NHC carbene ligand-based Cp*Ir catalyst (C-25) for CO₂ hydrogenation at ambient pressure and FA dehydrogenation at low temperature.²⁵ They demonstrated the hydrogenation of CO₂ to formate using 1 atm of CO₂ and H₂ at 30 °C to obtain a TOF of 44 h⁻¹, where initially they bubbled CO₂ (70 mL/min) into an aqueous KOH (1 M) solution of C-25, followed by passing CO₂ and H₂ with a rate of 70 mL/min simultaneously for an extra hour at 30 °C. Reducing the catalyst amount resulted in an increase in the TOF value to 58 h⁻¹. According to the plausible catalytic cycle, C-25 cleaves H₂ to produce Ir–H species in basic conditions at a pH of ~8.5, where Ir–H species hydrogenated CO₂ (or bicarbonate) to produce HCO₂⁻ and subsequently the Ir-formate species. Further, when the Ir-formate species was treated with KOH, formate was released with the regeneration of the active form of catalyst C-25. In the dehydrogenation process, using C-25 as the catalyst in a 5:2 mixture of HCO₂H and NEt₃ at 90 °C resulted in a TOF of 58 000 h⁻¹ in 2 min (pH 3.7). Carrying out further reactions in a larger volume (4.5 mL) under analogous reaction conditions resulted in an increased TOF value of 96 000 h⁻¹. Further, in a multiple-charging experiment, the highest TOF of 100 000 h⁻¹ was achieved at 90 °C (pH 4.4) using a 1 M FA/HCOONa solution. Hence, C-25 was found to be active for both H₂-storage and release processes using the CO₂/FA system. The observed activity was attributed to the imidazolylidene-based abnormal NHC ligand, a proton-responsive ligand framework enabling protonation during the dehydrogenation process. This was facilitated by the proton transfer and strong σ-donating ability of the abnormal NHC backbone to the enhanced electron density required during hydrogenation/

dehydrogenation steps. Additionally, the robust bonding between iridium and the abnormal NHC ligand ensures structural stability.

Fidalgo et al. developed Cp*Ir (C-26) and Cp*Rh (C-27) catalysts bearing an 8-aminoquinoline ligand for the catalytic CO₂ hydrogenation and FA dehydrogenation.²⁶ Initially, CO₂ hydrogenation was performed in an aqueous KOH solution under 10 bar p_{H₂}/p_{CO₂} (1:1) at 80 °C for 8 h, where TONs of 6021 and 5991 was achieved in the presence of C-26 and C-27, respectively. Further, when the time and temperature were decreased to 3 h and 40 °C, respectively, the TON slightly decreased to 5662 in the case of C-26 and no formate yield was observed in the case of C-27, implying that the Cp*Ir complex (C-26) is more active than the Cp*Rh complex (C-27). Similarly, FA dehydrogenation reactions were performed with Cp*Ir (C-26) and Cp*Rh (C-27) catalysts in water. At an initial pH of 4.5, the C-26 (0.04 mol %) catalyst achieved a TON of 3109 and the C-27 (0.04 mol %) catalyst achieved a TON of 2109 when a mixture of FA/HCOONa (1:2) was refluxed at 100 °C in water. Additionally, the presence of the umpolung process was inferred when D₂O was used instead of H₂O where the interaction of D⁺ with the Ir–H group takes place, resulting in the formation of [Cp*Ir(HD)-(8-aminoquinoline)]²⁺. Further, the mechanistic study revealed that the coordination of the NH₂ group to the metal center had a positive effect on the reaction by assisting the proton transfer to the Ir-hydrido group.

Later, Kanega et al. reported Cp*Ir catalysts (C-28–C-33) containing deprotonated pyridylamide-based ligands for CO₂ hydrogenation and FA dehydrogenation (Scheme 7).²⁷ They proposed that the higher catalytic activity of these catalysts for CO₂ hydrogenation and FA dehydrogenation was due the strong capability of the coordinated anionic nitrogen atom for electron donation and the proton-responsive nature of the OH group close to the metal center. First, CO₂ hydrogenation was investigated using Cp*Ir catalysts with varying pyridylamide ligands under a 1:1 ratio of p_{H₂}/p_{CO₂} (1.0 MPa) with 1 M NaHCO₃ at 50 °C at pH of 8.2. Among them, Cp*Ir containing a picolinamidate catalyst (C-28) exhibited a TOF of 1230 h⁻¹, ascribed to the formation of anionic species and distribution of electron density on the coordinated N atom. Further, the Cp*Ir catalyst (C-30) having OH groups at the *ortho* positions of the pyridine ring of C-29 significantly enhanced the catalytic activity by exhibiting the highest TOF value of 3140 h⁻¹. The Cp*Ir catalyst with an imidazoline-based ligand (C-31) exhibited a high TOF of 2080 h⁻¹. On the other hand, when CO₂ hydrogenation was performed at 25 °C using 1.0 M NaHCO₃ using 0.1 MPa p_{H₂}/p_{CO₂} (1:1) at pH 8.2, C-30 exhibited the highest TOF of 198 h⁻¹. The catalyst C-30 was also found to be durable, exhibiting a TON of 655

Scheme 8. Catalytic CO₂ Hydrogenation and FA Dehydrogenation over the Catalyst C-34^{4f}

^{4f}Reprinted with permission from ref 28. Copyright 2015 American Chemical Society.

after 3 days. On the other hand, C-32 having *para*-substituted OH on the pyridyl group exhibited the highest TON (14700) and formate concentration (0.643 M). For FA dehydrogenation, the Cp^{*}Ir catalyst having an *N*-phenyl-picolinamidate ligand without an OH group (C-29) showed a TOF of 11 800 h⁻¹ at 60 °C at pH 3.5. The catalyst activity trend observed for CO₂ hydrogenation was not followed for FA dehydrogenation, which was attributed to the stability of catalysts in acidic conditions. However, introducing phenyl groups on the amido-N significantly improved the activity of the catalysts (TOF = 61 700 h⁻¹ over C-29) in a 1 M FA/HCOONa (9:1) solution. Cp^{*}Ir catalysts with hydroxyl (OH) groups on the pyridine ring (C-32 and C-30) could not show any significant improvement in the catalytic activity. Among imidazole-, imidazoline-, and pyrazole-based Cp^{*}Ir catalysts, the imidazole-based Cp^{*}Ir catalyst (C-33) exhibited a TOF of 30 100 h⁻¹. Overall, the FA dehydrogenation rates were pH-dependent, and the durability of some of the catalysts in 1 M FA solutions was found to be low. After evaluating a set of catalysts, the authors analyzed the pH dependence of their catalytic activities in FA dehydrogenation. Substitutions on the amide-N were found to have a stronger impact on the pH-dependence and catalytic activity than OH groups substituted on the pyridine rings. Among the catalysts explored, C-29 showed increased activity with increasing FA concentration and achieved complete conversion of FA at 6 M. The rate of gas release was stable, and the TOF reached 11 800 h⁻¹ in an 8 M FA/HCOONa (9:1) solution at 60 °C. The durability of C-29 was also found to be higher, where almost complete consumption of FA and release of 51 L of mixed gases were observed in 100 h. The kinetic isotopic effect (KIE) results inferred that DCOOD exerted a greater effect than D₂O, and

hence the β-hydride elimination step to produce Ir–H and CO₂ is the rate-determining step.

Mo et al. developed a Cp^{*}Ir catalyst based on a proton-responsive N₂N pyridyl pyrrole ligand [Cp^{*}Ir(N₂N X)]ⁿ⁺ (Cp^{*} = pentamethylcyclopentadiene; X = Cl, *n* = 0; X = H₂O, *n* = 1) for reversible CO₂ hydrogenation and FA dehydrogenation.²⁸ The catalyst C-34 exhibited exceptional performance for CO₂ hydrogenation in an aqueous solution at ambient 1 bar *p*H₂/*p*CO₂ (1:1) at 25 °C, with a TOF of 4.5 h⁻¹. The TOF significantly increased to 29 h⁻¹ when MeOH/H₂O (1.5:1) was used to enhance the catalyst solubility and reactivity. The outstanding catalytic performance of C-34 can be attributed to several factors, primarily the cooperative effect of the metal–ligand system, particularly the pyrrole group in the complex. The pyrrole group facilitates cooperative heterolytic H–H bond cleavage during CO₂ hydrogenation and accepts a proton in FA dehydrogenation (Scheme 8). Initially, the CsOH base was employed for hydrogenation, as it generates bicarbonate *in situ* during the catalytic process. Exploring other carbonate and bicarbonate bases results in the formation of formate, even in the absence of CO₂. Furthermore, the catalyst could not catalyze the hydrogenation of CO₂ in the presence of weak bases (NH₃, DBU, and TEOA). The reversible H₂ storage capability of the catalyst could be controlled by tuning the reaction pH. The pyrrole group, sensitive to protons, acquires a proton from H₂O and loses one to OH⁻, as the water bridge serves as a proton channel. The catalyst C-34 also demonstrated good catalytic activity for additive-free FA dehydrogenation, achieving a maximum TOF of 45 900 h⁻¹ at 90 °C in water compared to that observed in neat FA. A catalytic dinuclear hydride intermediate was proposed to be involved in the catalytic FA

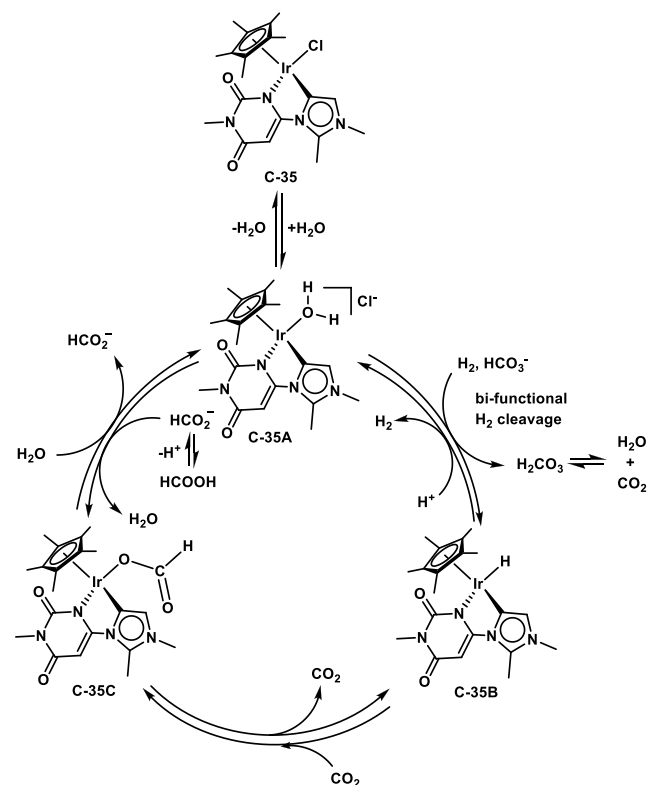
dehydrogenation. The cooperative effect of the ligand and the Ir metal in the catalyst C-34 contributed to the observed high catalytic performance, where during FA dehydrogenation the pyrrole group accepts a proton from FA. At the same time, during CO₂ hydrogenation, pyrrole assists in the cooperative heterolytic cleavage of H–H bond. The pH of the reaction played a crucial role, where the pH was tuned by the FA/HCOONa ratio in the FA dehydrogenation reaction, with fixed concentrations of FA and HCOONa at 2 M. At a pH of 1.81, higher activity was observed for FA dehydrogenation, achieving a maximum TOF of 45 900 h⁻¹. Further increasing the pH resulted in a decreased catalytic activity, while the reaction rate increased at higher reaction temperatures.

Later in 2022, Maji et al. further explored a NHC-based Cp*Ir catalyst (C-35) for CO₂ hydrogenation and FA dehydrogenation in water in the absence of additives or solvents.²⁹ The catalyst C-35 exhibited a high TON of 16680 using 60 bar *p*H₂/*p*CO₂ (1:1) at 60 °C in 6 h. The observed prominent catalytic activity was attributed to the presence of the RN=C(=O) group, the σ -donor property of the NHC ligand, and the facile water solubility of the catalyst C-35. The pH analysis showed that the pH was initially 9.0 and subsequently dropped to 7.3, signifying the generation of bicarbonate as the reaction proceeds. To confirm this, the reduction of bicarbonate (HCO₃⁻) (KHCO₃, 5 mmol) was performed without additional CO₂ gas at 60 °C under 30 bar H₂ pressure for 1 h, resulting in a TON of 2100, while a TON of 3218 was obtained for CO₂ hydrogenation under analogous conditions. The catalyst C-35 also exhibited high activity for FA dehydrogenation, where a TOF of 70674 h⁻¹ was obtained at 80 °C within the first 5 min of the reaction. They concluded that the pH of the reaction mixture played a critical role in both the dehydrogenation and hydrogenation reactions (Scheme 9). A pH-switchable system for on-demand FA dehydrogenation was devised, where the pH of the reaction mixture could be adjusted to control the catalytic activity. Moreover, the evolved H₂ and CO₂ gases from the FA dehydrogenation reactions were successfully reutilized in the hydrogenation reaction, indicating the suitability of the C-35 catalytic system for utilizing FA as a typical H₂/CO₂ storage liquid. Additionally, the dehydrogenation of FA was found to be highly dependent on the pH of the reaction mixture; the maximum TON of 3600 h⁻¹ was obtained at pH 3.5, while lower activity was observed at pH 2.75. The CO₂ released from the FA dehydrogenation reaction was captured in KOH (1M) solution to hydrogenate it to formate with a TON of 20 over catalyst C-35. The authors further reutilized the H₂ and CO₂ gas that evolved from FA dehydrogenation for the hydrogenation of quinoxaline, resulting in an 88% yield of 1,2,3,4-tetrahydro quinoxaline at 50 °C in 1 h.

NON-NOBLE METAL-BASED MOLECULAR CATALYSTS

Unlike noble metal-based catalysts, non-noble metal-based molecular catalysts (Scheme 10) are less explored for reversible CO₂ hydrogenation and FA dehydrogenation (Table 1). Enthaler et al. reported a Ni-PCP-hydrido catalyst (C-36) that effectively catalyzed both FA dehydrogenation and bicarbonate hydrogenation to formate (Scheme 11).^{30a} The hydrogenation of NaHCO₃ to sodium formate with TON 3038 was achieved over C-36 at 55 bar H₂ pressure in methanol at 150 °C. Notably, the studied Ni-PCP catalyst demonstrated a reversible catalytic FA dehydrogenation/CO₂

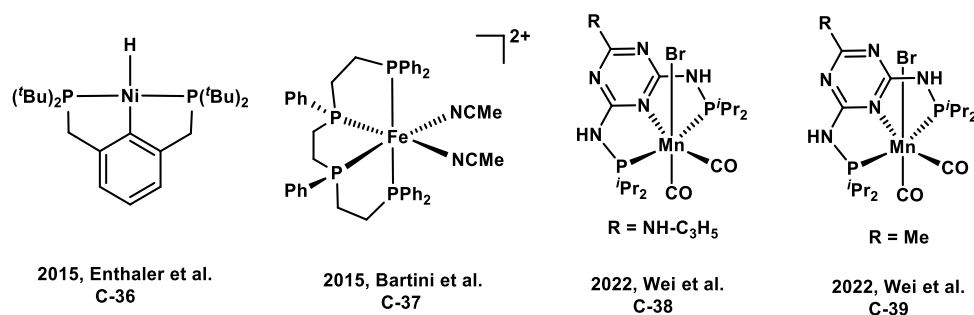
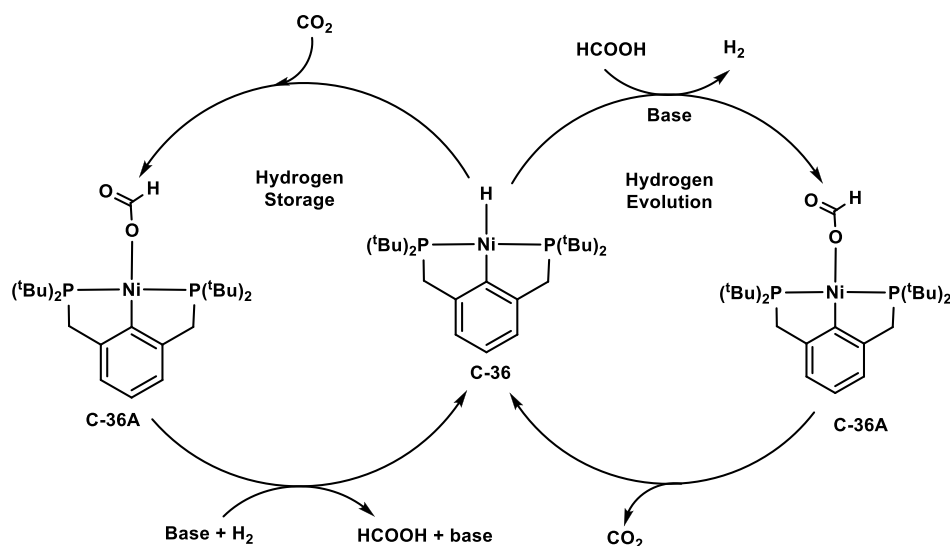
Scheme 9. Catalytic Cycle for Reversible CO₂ Hydrogenation and FA Dehydrogenation over the Catalyst C-35^a



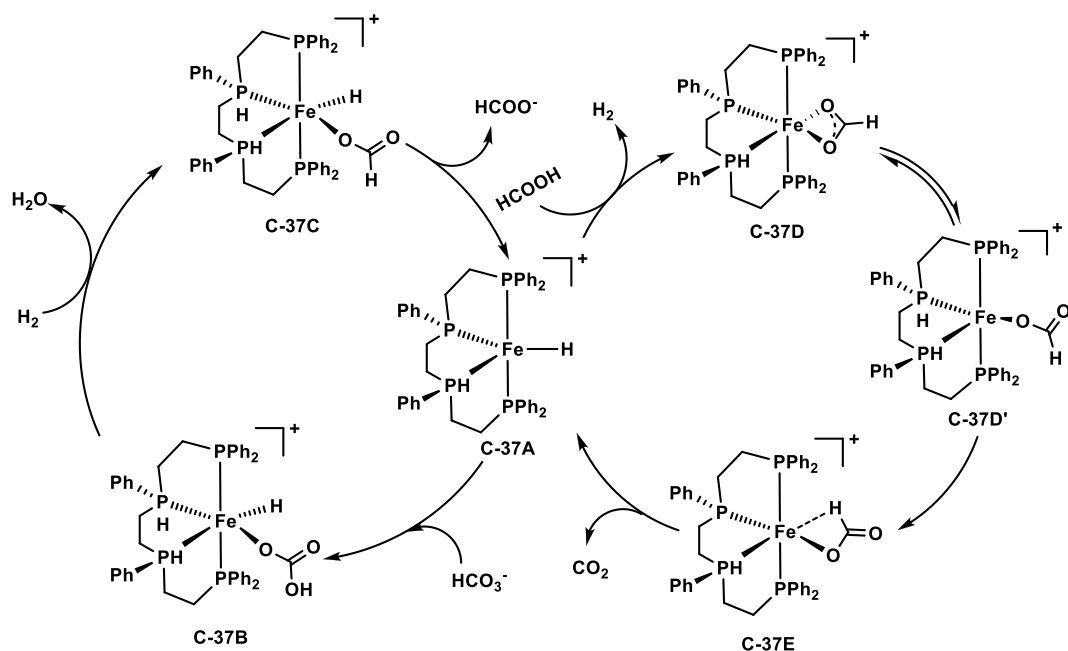
^aReprinted with permission from ref 29. Copyright 2022 American Chemical Society.

hydrogenation, wherein particularly Ni-PCP-hydrido (C-36) and Ni-PCP-formato species (C-36A) demonstrated high activity with TONs of 626 (for FA dehydrogenation using FA/NEt₃) and 3000 (for NaHCO₃ hydrogenation), respectively, at 80 °C in propylene carbonate solution.

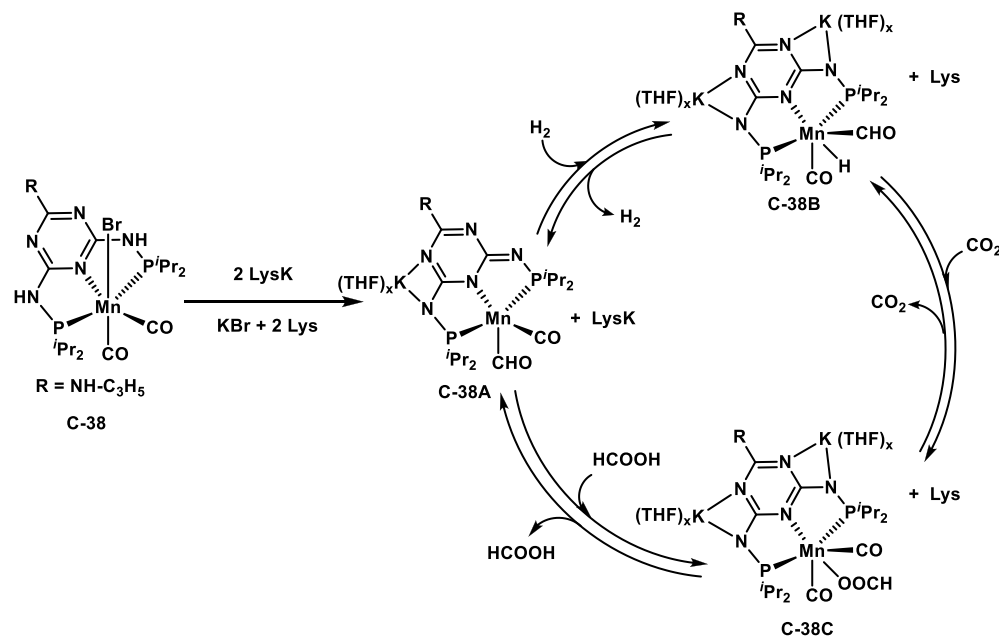
Bertini et al. developed an Fe (II) complex (C-37) for both bicarbonate hydrogenation and FA dehydrogenation. Sodium bicarbonate hydrogenation over the C-37 catalyst in MeOH under 60 bar H₂ yielded 76% formate with a TON of 762 at 80 °C.^{30b} Further, reducing the H₂ pressure to 30 bar resulted in a reduced formate yield (71%), albeit with a TON of 766 in 24 h. The authors proposed the Fe-hydrido species (C-37A) as the key intermediate in the observed catalytic activity, which utilized the availability of *cis* positions to undergo catalytic hydrogenation of bicarbonate via an inner-sphere mechanism (Scheme 12). On the other hand, FA dehydrogenation was performed over the *in situ* generated C-37 species using [Fe(CH₃CN)₆](BF₄)₂ with tetraphos (tetraphosphine 1,1,4,7,10,10-hexaphenyl-1,4,7,10-tetraphosphadecane) in propylene carbonate under base-free conditions, which resulted in considerably enhanced catalytic activity with initial TOF of 1737 h⁻¹ and a TON of 6061 in 6 h at 60 °C. Unlike bicarbonate hydrogenation, five-coordinate Fe species dominated the FA dehydrogenation reaction. Notably, the Fe-hydrido species (C-37A) was also found to play a crucial role in the catalytic FA dehydrogenation, where it facilitated the fast elimination of H₂ to regenerate the Fe-formato species (C-37D). The Fe-formato species underwent $\eta^2 \rightarrow \eta^1$ coordination shift and rearrangement, followed by β -hydride

Scheme 10. Non-Noble Metal-Based Catalysts C-36–C-39 Explored for Reversible CO₂ Hydrogenation and FA DehydrogenationScheme 11. Ni-PCP (C-36) Catalyzed Cyclic CO₂ Hydrogenation and FA Dehydrogenation System^{4a}

^{4a}Reprinted with permission from ref 30a. Copyright 2015 WILEY-VCH Verlag GmbH.

Scheme 12. Reaction Pathway for the Catalytic Hydrogenation of NaHCO₃ and FA Dehydrogenation over C37A^{4b}

^{4b}Reprinted with permission from ref 30b. Copyright 2015 American Chemical Society.

Scheme 13. Mn-PNP (C-38) Catalyzed CO₂ Hydrogenation and FA Dehydrogenation^a

^aReprinted with permission from ref 31a. Copyright 2022 Springer Nature Limited.

elimination, to form the Fe-hydrido species (C-37A) (Scheme 12).

Wei et al. employed a Mn-PNP catalyst (C-38) for reversible CO₂ hydrogenation and FA dehydrogenation.^{31a} The Mn-pincer complex (C-38) hydrogenated CO₂ to FA (88% yield) with a TON of 44 000 in the presence of lysine an α -amino acid using 20 bar CO₂ and 60 bar H₂ in H₂O/THF (1:1 v/v) at 145 °C for 12 h. Lowering the reaction temperature to 115 °C resulted in an increase in the formate yield to 92% with a TON of 230 000. In contrast, other bases and 16 amino acids exhibited lower formate yields, suggesting the significant role of lysine in the CO₂ hydrogenation process. The catalyst C-38 displayed high stability during the recyclability experiment for 10 consecutive runs, where 80% of initial productivity was retained to achieve a TON of 2 050 000. Further, the mechanistic investigation suggested that the addition of potassium lysine (LysK) to the catalyst resulted in the formation of a Mn-formyl species (C-38A), a possible catalytically active species. Further, pressurizing the reaction with H₂ (0.5 bar) gas resulted in the formation of Mn-hydrido species (C-38B) and subsequently the Mn-formato species (C-38C) with the addition of CO₂. For FA dehydrogenation, the Mn-PNP catalyst (C-38) exhibited good stability and reusability with high productivity, achieving a TON of 600 000. Further, in the presence of LysK, more than 80% H₂ evolution efficiency was achieved. Lowering the reaction temperature and using amino acids other than lysine resulted in a lower yield of H₂. Moreover, using other organic solvents, such as 2-methyl-THF, triglyme, and ethanol in FA/LysK mixtures, an ~88% yield of H₂ with more than 99% CO₂ retention was obtained because of the remarkable CO₂ capture properties of LysK. In order to understand the feasibility of reusing the catalyst and base, a biphasic solvent system was used to easily recycle the catalyst C-38 and the organic solvent, where >89% of the theoretical H₂ productivity for the FA dehydrogenation was achieved with a total TON of 676 700. Through their work, the authors demonstrated the applicability

of the Mn-PNP (C-38) catalyst for the reversible CO₂ hydrogenation and FA dehydrogenation (Scheme 13).

Wei et al. also reported a similar Mn-PNP catalyst with a methyl substituent (C-39) for the reversible hydrogenation of bicarbonate and carbonate and dehydrogenation of formate.^{31b} Hydrogenation of bicarbonate was performed in H₂O/THF (1:1 v/v) using H₂ gas (60 bar) at 90 °C to yield formate (95% yield) with a TON of 55000 in 12 h. Though the catalyst C-39 was not active for the hydrogenation of carbonate, performing the reaction using glutamic acid (as promotor) enhanced the activity to produce formate in an 82% yield, which was attributed to the CO₂ capturing properties of glutamic acid. Along with carbamate species (26%), bicarbonate (51%) and CO₂ (16%) were also formed when glutamic acid and K₂CO₃ were mixed. These findings show that glutamic acid has a substantial CO₂ capture impact and that a high yield in the carbonate-to-formate conversion depends on the synthesis of carbamate species. Moreover, C-39 also catalyzed the dehydrogenation of various formate salts (Li⁺, Na⁺, NH₄⁺, Cs⁺, Mg²⁺, and Ca²⁺) resulted in the generation of hydrogen gas with low purity (67–95%) in the absence of lysine. However, in the presence of lysine, high yields of H₂ (>91%) with high purity (>98%) was achieved. They further demonstrated the possibility of a stable hydrogen storage cycle by combining the processes of formate dehydrogenation and bicarbonate hydrogenation, with hydrogen being generated in an autoclave and collected using a buret, followed by hydrogen storage under pressure and repeating the dehydrogenation process in subsequent cycles.

■ FUTURE OUTLOOK

Formic acid (FA) has emerged as a promising hydrogen carrier for fuel cell applications. Several research groups have successfully demonstrated FA-based electricity generation, including the development of model cars and power generators.⁴ Despite the fact that FA has 4.4 wt % of H₂ content, H₂ produced from FA releases an equimolar amount

of CO₂, which is not considered an environmentally green process. However, with the development of an efficient CO₂-to-FA conversion process, the cyclic FA dehydrogenation and CO₂ hydrogenation process has emerged as promising carbon-neutral pathway. Although several homogeneous catalysts have been reported separately for FA dehydrogenation and CO₂ hydrogenation, the development of an efficient catalytic system that can catalyze both FA dehydrogenation and CO₂ hydrogenation over the same catalytic system is highly desirable.^{5c}

Catalyst efficiency, energy consumption, scalability, and overall process economics are still challenges that need to be addressed for bulk-scale FA dehydrogenation and CO₂ hydrogenation. It is supposed that a moderate TOF of 5000–10 000 h⁻¹ is considered sufficient for onboard applications.⁴ To improve the economic viability of the process, there is a need to development of new catalysts that can provide a maximum TON.⁴ Benchmarking the catalytic performance is indeed crucial for assessing the potential of a catalyst. The catalyst should be cost-effective, enabling its usage for bulk-scale processes. The catalyst must exhibit high activity and selectivity in producing the desired product, avoiding other side reactions with unwanted byproducts. It must also possess high stability and recyclability for long-term usage. For example, catalysts with proton-responsive ligands assist in anchoring CO₂ molecules when they are in close proximity, thereby activating CO₂ molecules for hydrogenation. This can lead to more efficient catalysis, as proton transfer steps are often rate-limiting. They can assist in the transfer of protons from FA to the metal center, facilitating the dehydrogenation process. Further, the reactions can be tuned (CO₂ hydrogenation/FA dehydrogenation) by varying the pH of the reaction conditions. These ligands can help stabilize the catalyst under varying pH conditions, maintaining its activity and preventing catalyst deactivation due to harsh reaction conditions. The concept of utilizing a pH switch to store and release hydrogen gas is an idea that holds potential advantages for hydrogen storage systems. However, it is crucial to consider the hurdles, including the buffering effect. The pH-dependent system has the potential to enable the controlled storage and release of hydrogen gas, which is essential for applications where efficient storage and on-demand release of hydrogen are required. Additionally, by manipulating the pH of the system, it might be possible to regulate the rate at which hydrogen is released, offering flexibility in meeting varying demands for hydrogen. Additionally, repeated cycles of operation can result in a buffered pH in the system due to the accumulation of basic byproducts. This can hinder the storage and release of hydrogen and might hamper its practical application. Therefore, additional steps must be taken to recalibrate or reset the pH, thereby bringing back the effectiveness of the catalytic system and its ability to rapidly adsorb and release hydrogen. Using reversible technology for FA dehydrogenation and CO₂ hydrogenation, it is possible to make the system environmentally friendly. The process of producing FA from the hydrogenation of carbon dioxide (CO₂) needs to be more energy efficient. Hence, the development of a catalytic system that can reversibly accomplish highly effective reactions that store hydrogen by hydrogenating the medium and extracting hydrogen by dehydrogenation will be the most crucial component of hydrogen storage systems.^{5c} This step is crucial for utilizing CO₂ as a feedstock for hydrogen storage and reducing carbon emissions. Substantial engineering efforts are

required to assess the potential and limitations of future improvements in reversible dehydrogenation and hydrogenation processes. The concept of reversible FA dehydrogenation (producing hydrogen) and CO₂ hydrogenation (producing FA) systems holds promise for a sustainable hydrogen energy future.

CONCLUSION

In this Review, various transition metal-based molecular catalysts have been extensively discussed for their catalytic performance for the reversible CO₂ hydrogenation and FA dehydrogenation-based H₂ storage–release cycle. A hydrogen-on-demand system is made possible by the conversion of hydrogen and formic acid, in which hydrogen is stored as FA and is produced through a catalytic breakdown when required. Reports revealed the crucial role of pH-responsive ligands in achieving high catalytic activity for reversible CO₂ hydrogenation and FA dehydrogenation over the same catalytic system. For instance, catalysts such as C-11, having ligands with hydroxy (–OH) groups, exhibited considerably higher activity compared to those containing methoxy (–OMe) substituents, owing to both electronic and pendent base effects of –OH or –O⁻ in facilitating H₂ heterolysis. Additionally, the position of substituents on the pyridine moiety greatly influenced the initial catalytic rate, with the *ortho* position resulting in better hydrogenation activity than the *para* position. The best catalytic activity was observed when two hydroxy (–OH) groups were present at the *ortho* and *para* positions on the pyridine ring. However, replacing the pyridine moiety with a pyrimidine ring led to a significant decrease in the catalytic activity, highlighting the impact of the ligand. The study also introduces a new approach of using an imidazolylidene-based strongly σ -donating abnormal NHC ligand in conjunction with a proton-responsive ligand framework, which can have dual activity toward the chemical hydrogen storage/delivery process. Further, due to the metal–ligand cooperative effect, complexes show extraordinary catalytic performance. The pyrrole group, which accepts a proton from FA added in the dehydrogenation reaction, shows a metal–ligand cooperative effect and in the CO₂ hydrogenation assists with cooperative heterolytic H–H bond cleavage. It is also evident from these reports that, despite the higher activity of Ir-based catalysts for CO₂ hydrogenation and FA dehydrogenation, the development of Ru-based systems has gained significant attention as a highly active low-cost substitute for Ir-based catalysts. Several Ru-pincer, (arene)Ru, and Cp*Ir based catalytic systems have been extensively explored as potentially active catalytic systems for achieving reversible CO₂ hydrogenation and FA dehydrogenation. Moreover, non-noble metal-based molecular catalysts are also gaining attention.

Overall, these reports suggested that indeed the formic acid-based system has the potential to significantly contribute to the future of the hydrogen economy. Establishing a CO₂/FA-based H₂ storage/release system may have significant impact on the global effects toward reducing greenhouse gas emissions and mitigating climate change issues. Further, (bi)carbonates and formate salts could be the preferred choice over the conventional carbon dioxide/FA pair for the storage and handling of hydrogen. Hence, the CO₂/(bi)carbonate-formic acid system lays the foundation for developing a chemical hydrogen storage and release, utilizing environmentally benign and economical catalysts and solvent systems

for achieving a carbon-neutral future. It is therefore important to view the current challenges as opportunities for innovation and advancement in hydrogen production and storage technologies. By addressing these challenges, the cyclic FA dehydrogenation-CO₂ hydrogenation-based system can be realized as a more sustainable process for the H₂ storage and release in future.^{4,5}

AUTHOR INFORMATION

Corresponding Author

Sanjay Kumar Singh – Catalysis Group, Department of Chemistry, Indian Institute of Technology Indore, Indore 453552 Madhya Pradesh, India; orcid.org/0000-0002-8070-7350; Email: sksingh@iiti.ac.in

Authors

Sanjeev Kushwaha – Catalysis Group, Department of Chemistry, Indian Institute of Technology Indore, Indore 453552 Madhya Pradesh, India

Jayashree Parthiban – Catalysis Group, Department of Chemistry, Indian Institute of Technology Indore, Indore 453552 Madhya Pradesh, India

Complete contact information is available at:
<https://pubs.acs.org/10.1021/acsomega.3c05286>

Author Contributions

[†]Authors with equal contribution.

Notes

The authors declare no competing financial interest.

Biographies



Sanjeev Kushwaha received his B.Sc. in Chemistry in 2016 from Lucknow University, India, and subsequently received his M.Sc. in Chemistry in 2018 from the same institution. Then, he joined the catalysis group, Department of Chemistry, Indian Institute of Technology, Indore, India, in 2019 as a Ph.D. student under the supervision of Prof. Sanjay Kumar Singh. His research expertise focuses on the development of active molecular catalysts for hydrogen production from C-1-based LOHCs. He is currently working on hydrogen production from formic acid.



Jayashree Parthiban received her Integrated M.Sc. in Chemistry in 2019 from Central University of Tamil Nadu, India. She joined the catalysis group, Department of Chemistry, Indian Institute of Technology, Indore, India, in 2021 as a Ph.D. student under the supervision of Prof. Sanjay Kumar Singh. Her research expertise involves the synthesis of metal catalysts for C-1 substrate hydrogenation. She is currently working on CO₂ capture and conversion.



Sanjay Kumar Singh obtained his Ph.D. in Chemistry from A.P.S. University, Rewa, India. He had consecutive postdoctoral stays at AIST, Osaka, Japan (as a JSPS postdoctoral fellow and later as AIST postdoctoral scientist with Prof. Qiang Xu) and at Karlsruhe Institute of Technology, Karlsruhe, Germany (as Alexander von Humboldt postdoctoral fellow with Prof. Peter W. Roesky). In 2012, he joined the Indian Institute of Technology Indore, India, as an Assistant Professor in Chemistry, and since February 2022 he has been a Professor at the same institution. His research focuses on the design and development of new and efficient catalysts and materials for CO₂ capture and conversion, hydrogen production and storage, and biomass/waste transformation to value-added chemicals and fuels.

ACKNOWLEDGMENTS

The authors acknowledge the financial support received from IIT Indore, DST-SERB (CRG/2021/000504) and CSIR (01(3045)/21/EMR-II), New Delhi, India. S.K. and J.P. thank INSPIRE, DST, New Delhi, India, and CSIR, New Delhi, India, respectively, for their fellowships.

REFERENCES

- (1) (a) Global Monitoring Laboratory. *Trends in atmospheric carbon dioxide*; National Oceanic and Atmospheric Administration: Washington, D.C., n.d. <https://gml.noaa.gov/ccgg/trends/> (accessed 2022-07-1). (b) Friedlingstein, P.; O'Sullivan, M.; Jones, M. W.; Andrew, R. M.; Gregor, L.; Hauck, J.; Le Quéré, C.; Luijckx, I. T.; Olsen, A.; Peters, G. P.; Peters, W.; Pongratz, J.; Schwingshackl, C.; Sitch, S.;

- Canadell, J. G.; Ciais, P.; Jackson, R. B.; Alin, S. R.; Alkama, R.; Arneth, A.; Arora, V. K.; Bates, N. R.; Becker, M.; Bellouin, N.; Bittig, H. C.; Bopp, L.; Chevallier, F.; Chini, L. P.; Cronin, M.; Evans, W.; Falk, S.; Feely, R. A.; Gasser, T.; Gehlen, M.; Gkritzalis, T.; Gloege, L.; Grassi, G.; Gruber, N.; Gürses, Ö.; Harris, I.; Hefner, M.; Houghton, R. A.; Hurtt, G. C.; Iida, Y.; Ilyina, T.; Jain, A. K.; Jersild, A.; Kadono, K.; Kato, E.; Kennedy, D.; Klein Goldewijk, K.; Knauer, J.; Korsbakken, J. I.; Landschützer, P.; Lefevre, N.; Lindsay, K.; Liu, J.; Liu, Z.; Marland, G.; Mayot, N.; McGrath, M. J.; Metz, N.; Monacchi, N. M.; Munro, D. R.; Nakaoka, S. I.; Niwa, Y.; O'Brien, K.; Ono, T.; Palmer, P. I.; Pan, N.; Pierrot, D.; Pockock, K.; Poulter, B.; Resplandy, L.; Robertson, E.; Rödenbeck, C.; Rodriguez, C.; Rosan, T. M.; Schwinger, J.; Séférian, R.; Shutler, J. D.; Skjelvan, I.; Steinhoff, T.; Sun, Q.; Sutton, A. J.; Sweeney, C.; Takao, S.; Tanhua, T.; Tans, P. P.; Tian, X.; Tian, H.; Tilbrook, B.; Tsujino, H.; Tubiello, F.; van der Werf, G. R.; Walker, A. P.; Wanninkhof, R.; Whitehead, C.; Willstrand Wranne, A.; Wright, R.; Yuan, W.; Yue, C.; Yue, X.; Zaehle, S.; Zeng, J.; Zheng, B. Global carbon budget 2022. *Earth Syst. Sci. Data* **2022**, *14*, 4811–4900. (c) Keeling, C. D.; Harris, T. B.; Wilkins, E. M. Concentration of atmospheric carbon dioxide at 500 and 700 mbar. *J. Geophys. Res.* **1968**, *73*, 4511–4528. (d) Broken Record: Atmospheric Carbon Dioxide Levels Jump Again. *National Oceanic and Atmospheric Administration*, July 5, 2023. <https://www.noaa.gov/news-release/broken-record-atmospheric-carbon-dioxide-levels-jump-a-g-a-i-n#:~:text=Carbon%20dioxide%20levels%20measured%20at,of%20California%20San%20Diego%20announced.> (accessed 2023-07-05). (d) Lindsey, R. Climate Change: Atmospheric Carbon Dioxide. *Climate.gov*, May 12, 2023. <https://www.climate.gov/news-features/understanding-climate/climate-change-atmospheric-carbon-dioxide>, (accessed 2023-07-05). (e) Nocito, F.; Dibenedetto, A. Atmospheric CO₂ Mitigation Technologies: Carbon Capture Utilization and Storage. *Green Sustainable Chem.* **2020**, *21*, 34–43. (f) Kar, S.; Goepfert, A.; Prakash, G. K. S. Integrated CO₂ Capture and Conversion to Formate and Methanol: Connecting Two Threads. *Acc. Chem. Res.* **2019**, *52*, 2892–2903. (g) *Carbon Dioxide Utilisation: Closing the Carbon Cycle*, 1st ed.; Styring, P., Quadrelli, E. A., Armstrong, K., Eds.; Elsevier, 2015. (h) Centi, G.; Iaquaniello, G.; Perathoner, S. Can We Afford to Waste Carbon Dioxide? Carbon Dioxide as a Valuable Source of Carbon for the Production of Light Olefins. *ChemSusChem* **2011**, *4*, 1265–1273. (i) Olah, G. A.; Prakash, G. K. S.; Goepfert, A. Anthropogenic Chemical Carbon Cycle for a Sustainable Future. *J. Am. Chem. Soc.* **2011**, *133*, 12881–12898.
- (2) (a) *Chemical Transformations of Carbon Dioxide*; Wu, X. F., Beller, M., Eds.; Topics in Current Chemistry Collections; Springer, 2018. (b) Scott, M.; Blas Molinos, B.; Westhues, C.; Franciò, G.; Leitner, W. Aqueous Biphasic Systems for the Synthesis of Formates by Catalytic CO₂ Hydrogenation: Integrated Reaction and Catalyst Separation for CO₂-Scrubbing Solutions. *ChemCatChem* **2017**, *10*, 1085–1093. (c) Aresta, M.; Dibenedetto, A.; Angelini, A. Catalysis for the Valorization of Exhaust Carbon: from CO₂ to Chemicals, Materials, and Fuels. Technological Use of CO₂. *Chem. Rev.* **2014**, *114*, 1709–1742. (d) Peters, M.; Koehler, B.; Kuckshinrichs, W.; Leitner, W.; Markewitz, P.; Mueller, T. E. Chemical Technologies for Exploiting and Recycling Carbon Dioxide into the Value Chain. *ChemSusChem* **2011**, *4*, 1216–1240. (e) Benson, E. E.; Kubiak, C. P.; Sathrum, A. J.; Smieja, J. M. Electrocatalytic and Homogeneous Approaches to Conversion of CO₂ to Liquid Fuels. *Chem. Soc. Rev.* **2009**, *38*, 89–99. (f) Aresta, M.; Dibenedetto, A. Utilisation of CO₂ as a Chemical Feedstock: Opportunities and Challenges. *Dalton Trans.* **2007**, 2975–2992.
- (3) (a) Hietala, J.; Vuori, A.; Johnsson, P.; Pollari, I.; Reutemann, W.; Kieczka, H. Formic Acid. *Ullmann's Encyclopedia of Industrial Chemistry* **2016**, DOI: 10.1002/14356007.a12_013.pub3. (b) Tanaka, R.; Yamashita, M.; Chung, L. W.; Morokuma, K.; Nozaki, K. Mechanistic Studies on the Reversible Hydrogenation of Carbon Dioxide Catalyzed by an Ir-PNP Complex. *Organometallics*. **2011**, *30*, 6742–6750.
- (4) Guan, C.; Pan, Y.; Zhang, T.; Ajitha, M. J.; Huang, K. W. An update on formic acid Dehydrogenation by Homogeneous Catalysis. *Chem. Asian J.* **2020**, *15*, 937–946.
- (5) (a) Felderhoff, M.; Weidenthaler, C.; von Helmolt, R.; Eberle, U. Hydrogen storage: the remaining scientific and technological challenges. *Phys. Chem. Chem. Phys.* **2007**, *9*, 2643–2653. (b) Armaroli, N.; Balzani, V. The hydrogen issue. *ChemSusChem* **2011**, *4*, 21–36. (c) Shimbayashi, T.; Fujita, K. Metal-catalyzed hydrogenation and dehydrogenation reactions for efficient hydrogen storage. *Tetrahedron* **2020**, *76* (11), No. 130946.
- (6) EFSA FEEDAP Panel (EFSA Panel on Additives and Products or Substances used in Animal Feed). Scientific Opinion on the safety and efficacy of formic acid when used as a technological additive for all animal species. *EFSA J.* **2014**, *12* (10), 3827.
- (7) (a) Iguchi, M.; Himeda, Y.; Manaka, Y.; Matsuoka, K.; Kawanami, H. Kinetic studies of formic acid dehydrogenation catalyzed by an iridium complex towards insights into the catalytic mechanism of high-pressure hydrogen gas production. *ChemCatChem*. **2016**, *8*, 886–890. (b) Guan, C.; Zhang, D.; Pan, Y.; Iguchi, M.; Ajitha, M. J.; Hu, J.; Li, H.; Yao, C.; Huang, M.; Min, S.; Zheng, J.; Himeda, Y.; Kawanami, H.; Huang, K. Dehydrogenation of Formic Acid Catalyzed by a Ruthenium Complex with an N, N'-Diimine Ligand. *Inorg. Chem.* **2017**, *56*, 438–445. (c) Patra, S.; Maji, B.; Kawanami, H.; Himeda, Y. *RSC Sustain.* **2023**, DOI: 10.1039/D3SU00149K.
- (8) (a) Fukuzumi, S. Bioinspired energy conversion systems for hydrogen production and storage. *Eur. J. Inorg. Chem.* **2008**, *2008*, 1351–1362. (b) Enthaler, S.; Von Langermann, J.; Schmidt, T. Carbon dioxide and Formic acid—the couple for environmental-friendly hydrogen storage? *Energy Environ. Sci.* **2010**, *3*, 1207–1217. (c) Johnson, T. C.; Morris, D. J.; Wills, M. Hydrogen generation from formic acid and alcohols using homogeneous catalysts. *Chem. Soc. Rev.* **2010**, *39*, 81–88. (d) Loges, B.; Boddien, A.; Gärtner, F.; Junge, H.; Beller, M. Catalytic Generation of Hydrogen from formic acid and its Derivatives: Useful Hydrogen Storage Materials. *Top. Catal.* **2010**, *53*, 902–914. (e) Fukuzumi, S.; Yamada, Y.; Suenobu, T.; Ohkubo, K.; Kotani, H. Catalytic mechanisms of hydrogen evolution with homogeneous and heterogeneous catalysts. *Energy Environ. Sci.* **2011**, *4*, 2754–2766. (f) Yadav, M.; Xu, Q. Liquid-phase chemical hydrogen storage materials. *Energy Environ. Sci.* **2012**, *5*, 9698–9725. (g) Wang, W. H.; Himeda, Y.; Muckerman, J. T.; Manbeck, G. F.; Fujita, E. CO₂ Hydrogenation to Formate and Methanol as an Alternative to Photo and Electrochemical CO₂ Reduction. *Chem. Rev.* **2015**, *115*, 12936–12973. (h) Eppinger, J.; Huang, K. W. Formic acid as a Hydrogen Energy Carrier. *ACS Energy Lett.* **2017**, *2*, 188–195. (i) Singh, A. K.; Singh, S.; Kumar, A. Hydrogen energy future with formic acid: a renewable chemical hydrogen storage system. *Catal. Sci. Technol.* **2016**, *6*, 12–40. (j) Iglesias, M.; Oro, L. A. Mechanistic Considerations on Homogeneously Catalyzed Formic Acid Dehydrogenation. *Eur. J. Inorg. Chem.* **2018**, *2018*, 2125–2138. (k) Grasemann, M.; Laurenczy, G. Formic acid as a hydrogen source—recent developments and future trends. *Energy Environ. Sci.* **2012**, *5*, 8171–8181. (l) Mellmann, D.; Sponholz, P.; Junge, H.; Beller, M. Formic acid as a hydrogen storage material — development of homogeneous catalysts for selective hydrogen release. *Chem. Soc. Rev.* **2016**, *45*, 3954–3988.
- (9) (a) Zhou, X.; Huang, Y.; Xing, W.; Liu, C.; Liao, J.; Lu, T. High-quality hydrogen from the catalyzed decomposition of formic acid by Pd–Au/C and Pd–Ag/C. *Chem. Commun.* **2008**, 3540–3542. (b) Huang, Y.; Zhou, X.; Yin, M.; Liu, C.; Xing, W. Novel PdAu@Au/C Core–Shell Catalyst: Superior Activity and Selectivity in formic acid Decomposition for Hydrogen Generation. *Chem. Mater.* **2010**, *22*, 5122–5128.
- (10) (a) Iguchi, M.; Himeda, Y.; Manaka, Y.; Matsuoka, K.; Kawanami, H. Kinetic studies of formic acid dehydrogenation catalyzed by an iridium complex towards insights into the catalytic mechanism of high-pressure hydrogen gas production. *ChemCatChem*. **2016**, *8*, 886–890. (b) Iguchi, M.; Chatterjee, M.; Onishi, N.; Himeda, Y.; Kawanami, H. Sequential hydrogen production system

from formic acid and H₂/CO₂ separation under high-pressure conditions. *Sustain. Energy Fuels* **2018**, *2*, 1719–1725.

(11) Gao, Y.; Kuncheria, J. K.; Jenkins, H. A.; Puddephatt, R. J.; Yap, G. P. A. The interconversion of formic acid and hydrogen/carbon dioxide using a binuclear ruthenium complex catalyst. *Dalton Trans.* **2000**, *18*, 3212–3217.

(12) Man, M. L.; Zhou, Z. Y.; Ng, S. M.; Lau, C. P. Synthesis, characterization and reactivity of heterobimetallic complexes (η^5 -C₅R₅)Ru(CO)(μ -dppm)M(CO)₂(η^5 -C₅H₅) (R = H, CH₃; M = Mo, W). Interconversion of hydrogen/carbon dioxide and formic acid by these complexes. *Dalton trans.* **2003**, *19*, 3727–3735.

(13) Boddien, A.; Gärtner, F.; Federsel, C.; Sponholz, P.; Mellmann, D.; Jackstell, R.; Junge, H.; Beller, M. CO₂- "Neutral" Hydrogen Storage Based on Bicarbonates and Formates. *Angew. Chem., Int. Ed.* **2011**, *50*, 6411–6414.

(14) (a) Elek, J.; Nádasdi, L.; Papp, G.; Laurenczy, G.; Joó, F. Homogeneous Hydrogenation of Carbon Dioxide and Bicarbonate in Aqueous Solution Catalyzed by Water-Soluble Ruthenium(II) Phosphine Complexes. *Appl. Catal., A* **2003**, *255*, 59–67. (b) Papp, G.; Csorba, J.; Laurenczy, G.; Joó, F. A Charge/Discharge Device for Chemical Hydrogen Storage and Generation. *Angew. Chem., Int. Ed.* **2011**, *50*, 10433–10435.

(15) (a) Hsu, S. F.; Rommel, S.; Eversfield, P.; Müller, K.; Klemm, E.; Thiel, W. R.; Plietker, B. A Rechargeable Hydrogen Battery Based on Ru Catalysis. *Angew. Chem., Int. Ed.* **2014**, *53*, 7074–7078. (b) Filonenko, G. A.; Van Putten, R.; Schulpen, E. N.; Hensen, E. J. M.; Pidko, E. A. Highly Efficient Reversible Hydrogenation of Carbon Dioxide to Formates Using a Ruthenium PNP-Pincer Catalyst. *ChemCatChem* **2014**, *6*, 1526–1530.

(16) Kothandaraman, J.; Czaun, M.; Goepfert, A.; Haiges, R.; Jones, J. P.; May, R. B.; Prakash, G. K. S.; Olah, G. A. Amine-Free Reversible Hydrogen Storage in Formate Salts Catalyzed by Ruthenium Pincer Complex without pH Control or Solvent Change. *ChemSusChem* **2015**, *8*, 1442–1451.

(17) Xin, Z.; Zhang, J.; Sordakis, K.; Beller, M.; Du, C. X.; Laurenczy, G.; Li, Y. Towards Hydrogen Storage through an Efficient Ruthenium-Catalyzed Dehydrogenation of Formic Acid. *ChemSusChem* **2018**, *11*, 2077–2082.

(18) (a) Veron, R.; Puig, E.; Sutra, P.; Igau, A.; Fischmeister, C. Base-Free Reversible Hydrogen Storage Using a Tethered π -Coordinated-Phenoxy Ruthenium-Dimer Precatalyst. *ACS Catal.* **2023**, *13*, 5787–5794. (b) Piccirilli, L.; Rabell, B.; Padilla, R.; Riisager, A.; Das, S.; Nielsen, M. Versatile CO₂ Hydrogenation–Dehydrogenation Catalysis with a Ru–PNP/Ionic Liquid System. *J. Am. Chem. Soc.* **2023**, *145*, 5655–5663.

(19) Tanaka, R.; Yamashita, M.; Nozaki, K. Catalytic Hydrogenation of Carbon Dioxide Using Ir(III)-Pincer Complexes. *J. Am. Chem. Soc.* **2009**, *131*, 14168–14169.

(20) Himeda, Y.; Miyazawa, S.; Hirose, T. Interconversion between Formic Acid and H₂/CO₂ Using Rhodium and Ruthenium Catalysts for CO₂ Fixation and H₂ Storage. *ChemSusChem* **2011**, *4*, 487–493.

(21) Hull, J. F.; Himeda, Y.; Wang, W. H.; Hashiguchi, B.; Periana, R.; Szalda, D. J.; Muckerman, J. T.; Fujita, E. Reversible Hydrogen Storage Using CO₂ and a Proton-Switchable Iridium Catalyst in Aqueous Media under Mild Temperatures and Pressures. *Nat. Chem.* **2012**, *4*, 383–388.

(22) Maenaka, Y.; Suenobu, T.; Fukuzumi, S. Catalytic Interconversion between Hydrogen and Formic Acid at Ambient Temperature and Pressure. *Energy Environ. Sci.* **2012**, *5*, 7360–7367.

(23) Wang, L.; Onishi, N.; Murata, K.; Hirose, T.; Muckerman, J. T.; Fujita, E.; Himeda, Y. Efficient Hydrogen Storage and Production Using a Catalyst with an Imidazoline-Based, Proton-Responsive Ligand. *ChemSusChem* **2017**, *10*, 1071–1075.

(24) Siek, S.; Burks, D. B.; Gerlach, D. L.; Liang, G.; Tesh, J. M.; Thompson, C. R.; Qu, F.; Shankwitz, J. E.; Vasquez, R. M.; Chambers, N.; Szulcowski, G. J.; Grotjahn, D. B.; Webster, C. E.; Papish, E. T. Iridium and Ruthenium Complexes of N-Heterocyclic Carbene and Pyridinol-Derived Chelates as Catalysts for Aqueous Carbon Dioxide

Hydrogenation and Formic Acid Dehydrogenation: The Role of the Alkali Metal. *Organometallics* **2017**, *36*, 1091–1106.

(25) Semwal, S.; Kumar, A.; Choudhury, J. Iridium–NHC based catalyst for ambient pressure storage and low temperature release of H₂ via the CO₂/HCO₂H couple. *Catal. Sci. Technol.* **2018**, *8*, 6137–6142.

(26) Fidalgo, J.; Ruiz-Castañeda, M.; García-Herbosa, G.; Carbayo, A.; Jalón, F. A.; Rodríguez, A. M.; Manzano, B. R.; Espino, G. Versatile Rh- and Ir-Based Catalysts for CO₂ Hydrogenation, Formic Acid Dehydrogenation, and Transfer Hydrogenation of Quinolines. *Inorg. Chem.* **2018**, *57*, 14186–14198.

(27) Kanega, R.; Ertem, M. Z.; Onishi, N.; Szalda, D. J.; Fujita, E.; Himeda, Y. CO₂ Hydrogenation and Formic Acid Dehydrogenation Using Ir Catalysts with Amide-Based Ligands. *Organometallics* **2020**, *39*, 1519–1531.

(28) Mo, X. F.; Liu, C.; Chen, Z. W.; Ma, F.; He, P.; Yi, X. Y. Metal–Ligand Cooperation in Cp*Ir-Pyridylpyrrole Complexes: Rational Design and Catalytic Activity in Formic Acid Dehydrogenation and CO₂ Hydrogenation under Ambient Conditions. *Inorg. Chem.* **2021**, *60*, 16584–16592.

(29) Maji, B.; Kumar, A.; Bhattacharya, A.; Bera, J. K.; Choudhury, J. Cyclic Amide-Anchored NHC-Based Cp*Ir Catalysts for Bidirectional Hydrogenation–Dehydrogenation with CO₂/HCO₂H Couple. *Organometallics* **2022**, *41*, 3589–3599.

(30) (a) Enthaler, S.; Brück, A.; Kammer, A.; Junge, H.; Irran, E.; Güllak, S. Exploring the Reactivity of Nickel Pincer Complexes in the Decomposition of Formic Acid to CO₂/H₂ and the Hydrogenation of NaHCO₃ to HCOONa. *ChemCatChem* **2015**, *7*, 65–69. (b) Bertini, F.; Mellone, I.; Ienco, A.; Peruzzini, M.; Gonsalvi, L. Iron(II) Complexes of the Linear rac-Tetraphos-1 Ligand as Efficient Homogeneous Catalysts for Sodium Bicarbonate Hydrogenation and Formic Acid Dehydrogenation. *ACS Catal.* **2015**, *5*, 1254–1265.

(31) (a) Wei, D.; Sang, R.; Sponholz, P.; Junge, H.; Beller, M. Reversible hydrogenation of carbon dioxide to formic acid using a Mn-pincer complex in the presence of lysine. *Nat. Energy* **2022**, *7*, 438–447. (b) Wei, D.; Shi, X.; Sponholz, P.; Junge, H.; Beller, M. Manganese promoted (Bi) carbonate hydrogenation and formate dehydrogenation: Towards a circular carbon and hydrogen economy. *ACS Cent. Sci.* **2022**, *8*, 1457–1463.